



Article

Removal of Pb^{2+} , CrT, and Hg^{2+} Ions from Aqueous Solutions Using Amino-Functionalized Magnetic Nanoparticles

A. F. P. Allwin Mabes Raj^{1,2,3}, Maja Bauman¹, Marijana Lakić¹ , Nena Dimitrušev¹, Aleksandra Lobnik^{1,4} and Aljoša Košak^{1,4,*}

¹ IOS, Institute of Environmental Protection and Sensors, Ltd., Beloruska 7, SI-2000 Maribor, Slovenia

² Jožef Stefan International Postgraduate School, Jamova 39, 1000 Ljubljana, Slovenia

³ Department of Environmental Science, Jožef Stefan Institute, Jamova 39, 1000 Ljubljana, Slovenia

⁴ Faculty of Mechanical Engineering, Centre of Sensor Technology, University of Maribor, Smetanova 17, 2000 Maribor, Slovenia

* Correspondence: aljosa.kosak@um.si; Tel.: +386-5142-7567

Abstract: In this paper, a circular economy approach with the adsorption and desorption of heavy metal (HM) ions—i.e., lead (Pb^{2+}), chromium (CrT), and mercury (Hg^{2+})—from aqueous solutions was studied. Specific and selective binding of HM ions was performed on stabilized and amino-functionalized iron oxide magnetic nanoparticles ($\gamma\text{-Fe}_2\text{O}_3\text{@NH}_2$ NPs) from an aqueous solution at pH 4 and 7. For this purpose, $\gamma\text{-Fe}_2\text{O}_3\text{@NH}_2$ NPs were characterized by thermogravimetric analysis (TGA), Fourier-transform infrared spectroscopy (FTIR), specific surface area (BET), transmission electron microscopy (TEM), EDXS, and zeta potential measurements (ζ). The effects of different adsorbent amounts ($m_{\text{ads}} = 20/45/90$ mg) and the type of anions (NO_3^- , Cl^- , SO_4^{2-}) on adsorption efficiency were also tested. The desorption was performed with 0.1 M HNO_3 . The results showed improvement of adsorption efficiency for CrT, Pb^{2+} , and Hg^{2+} ions at pH 7 by 45 mg of $\gamma\text{-Fe}_2\text{O}_3\text{@NH}_2$ NPs, and the sequence was as follows: $\text{CrT} > \text{Hg}^{2+} > \text{Pb}^{2+}$, with adsorption capacities of 90.4 mg/g, 85.6 mg/g, and 83.6 mg/g, respectively. The desorption results showed the possibility for the reuse of $\gamma\text{-Fe}_2\text{O}_3\text{@NH}_2$ NPs with HNO_3 , as the desorption efficiency was 100% for Hg^{2+} ions, 96.7% for CrT, and 91.3% for Pb^{2+} .

Keywords: superparamagnetic nanoparticles; iron-oxide; maghemite; functionalization; aminopropyltrimethoxysilane; adsorption; desorption; lead; chromium; mercury; circular economy



Citation: Allwin Mabes Raj, A.F.P.; Bauman, M.; Lakić, M.; Dimitrušev, N.; Lobnik, A.; Košak, A. Removal of Pb^{2+} , CrT, and Hg^{2+} Ions from Aqueous Solutions Using Amino-Functionalized Magnetic Nanoparticles. *Int. J. Mol. Sci.* **2022**, *23*, 16186. <https://doi.org/10.3390/ijms232416186>

Academic Editor: Andreas Taubert

Received: 17 October 2022

Accepted: 30 November 2022

Published: 19 December 2022

Publisher's Note: MDPI stays neutral with regard to jurisdictional claims in published maps and institutional affiliations.



Copyright: © 2022 by the authors. Licensee MDPI, Basel, Switzerland. This article is an open access article distributed under the terms and conditions of the Creative Commons Attribution (CC BY) license (<https://creativecommons.org/licenses/by/4.0/>).

1. Introduction

Today, Europe is facing limited stocks of raw materials (RMs), such as heavy metal ions (HM ions) and rare-earth elements (REEs) [1–4]. Even more obviously, in the context of the COVID-19 pandemic, Europe's economy is facing an even larger lack of RMs and HM ions. Moreover, the European Union (EU)'s industry is dependent on imports of large amounts of RMs from the Asian market [1–3]. Therefore, the EU Commission was forced to prepare a list of critical raw materials (CRMs) [2,3,5,6], with sustainable strategies to foresee a circular economy based on recycling and reuse of critical REEs [2].

Lead (Pb^{2+}), chromium (total chromium (CrT)), and mercury (Hg^{2+}) ions are listed among the top 20 most hazardous substances [7,8] (accessed on 30 August 2022), since large amounts of HM ions are released into the environment due to agriculture and specific industries, such as the automotive, textile, mining, dye, and electroplating industries, among others [5,9–11]. HM ions dissolved in water are already toxic in small quantities and non-biodegradable, and some are carcinogenic and bioaccumulative, so they need to be treated as priority pollutants and efficiently cleaned [10–12].

Among these HMs, mercury has taken the spotlight because it is a global pollutant [13–16]. Mercury exists in various forms in the natural environment, such as mercurous (Hg_2^{+2}), and mercuric (Hg^{2+}), along with organic mercury-containing methyl and

ethyl groups. It is pertinent that the highly notorious form of methylmercury is caused by the methylation of inorganic [15] and elemental mercury [17] that is present in the aquatic environment by sulfate-reducing bacteria such as *Desulfovibrio desulfuricans*. Methylmercury can bioaccumulate and biomagnify in the oceanic food chain to reach 10^6 times the concentrations that have caused several tragedies in the past, such as the Minamata tragedy in Japan [15]. Negative toxic effects of versatile and highly mobile stable forms of chromium (Cr^{3+} and Cr^{6+}) are a constant threat to humans and the environment. Depending on the pH, they can be present in acidic media (pH 0–4) in the form of soluble complexes (Cr^{3+} , $[\text{Cr}(\text{H}_2\text{O})_6^{3+}]$), while near neutral (pH 6–9) inert precipitates ($\text{Cr}(\text{OH})_3(\text{s})$) can easily be adsorbed on solid media [18].

HM ions are present in different concentrations (trace and shock concentrations) and forms [19,20], in combined industrial and municipal wastewater streams. Disposal of treated wastewater into the environment necessitates adjusting its pH to neutral. Especially for recycling of HM ions and water reuse [19,21], this means raising costs and increases the complexity of the pretreatment process, as well as increasing the addition of excessive amounts of chemicals [19,21].

Therefore, it is necessary to act sustainably and environmentally consciously by removing HMs from the highly polluted wastewaters using technology/methods that allow the removal/recycling of HM ions [4].

Currently, different conventional methods are used to remove HM ions from water/industrial wastewater [5,11], such as precipitation [22], electrochemical removal [23], ion exchange [24], membrane filtration [25,26], coagulation [27], flocculation [28], and sorption on natural materials [29]. Although these methods are efficient in removing HM ions, they do not allow the recycling and reuse of HM ions. Some already well-established methods for the removal of HM ions produce toxic coproducts and large amounts of waste sludge [30], e.g., membrane filtration and coagulation/flocculation [31]. Moreover, these methods are often costly and energy-inefficient [30].

On the other hand, the adsorption method is well known, efficient, and used for the removal of HM ions due to its low adsorbent and operational costs and simple principle [5,11,12]. Adsorption can be performed with various natural materials [29] and other hybrid materials based on silica and iron oxide NPs ($\gamma\text{-Fe}_2\text{O}_3$, Fe_3O_4), as well as their functionalized forms [32–36]. The most commonly used adsorbent of HM ions from industrial and leachate wastewaters is activated carbon [31]. Activated carbon is efficient in the removal of HM ions from wastewaters, due to its high specific surface area, micropore volume, and pore volume [31,33,37–41]. At the same time, limitations of its use include non-selectivity and high material price. Furthermore, activated carbon does not enable the recycling and regeneration of HM ions and the adsorbent itself, and for now it does not enable the circular economy approach [31,33].

Due to the increased need for recycling of municipal and industrial wastewaters [42] research in nanotechnology is investing in the preparation and testing of functionalized (nano)materials that can improve the recycling of specific HM ions [34,36,43,44].

Maghemite ($\gamma\text{-Fe}_2\text{O}_3$) is a member of the family of iron oxides. It has a cubic spinel ferrite structure, and it is ferrimagnetic. When reduced to particle dimensions smaller than a certain domain—i.e., becoming a single domain—ferrimagnetic materials exhibit superparamagnetic behavior, which means that when an external magnetic field is applied, they magnetize, but when the magnetic field is removed, they no longer exhibit either residual magnetism or coercivity.

Such superparamagnetic nanoparticles, if they are surface-functionalized, provide promising applications in the adsorption of heavy metals from aqueous media, as they enable more efficient separation and recovery of heavy metals from the contaminated aqueous medium using an external magnetic field [45]. On the other hand, surface modification of superparamagnetic $\gamma\text{-Fe}_2\text{O}_3$ nanoparticles with TEOS and APTMS precursors improves their stability, prevents them from agglomerating, and increases their surface functionality by increasing the number of adsorption sites ($-\text{NH}_2$), facilitating and accelerating diffusion

pathways for heavy metal pollutants [46,47]. Despite all of the advantages of superparamagnetic γ -Fe₂O₃ nanocomposites for use in environmental technologies, the policy debate on their safety should not be ignored. Their toxicity is still an open question, even though much research has recently been carried out on this topic [48,49].

Surface functionalization of γ -Fe₂O₃ nanoparticles was performed via a sol-gel method involving base-catalyzed hydrolysis and co-condensation of tetra-coordinated alkoxy silanes in an alcohol medium. Tetra-coordinated silanes can be described by the general chemical formula R'_xSi(OR)_(4-x), 0 < x < 3, where OR is the hydrolyzable part (e.g., methoxy, ethoxy, etc.) and R' is the non-hydrolyzable part of the structure with functional substituents (e.g., amino, mercapto, carboxy, etc.).

Ideally, it would be expected that the 3-aminopropyltrimethoxysilane (APTMS, (CH₃O)₃-Si-(CH₂)₃-NH₂) molecules on the surface of the γ -Fe₂O₃ particles would polymerize into a highly homogeneous crosslinked SiO₂ coating with functional amino (-NH₂) groups present. However, the presence of a non-hydrolyzable fraction in the APTMS structure ((CH₃O)₃-Si-(CH₂)₃-NH₂) causes steric hindrance, and the electron density on the silicon (Si) atom increases due to the inductive (+I) effect, which decreases the rate of hydrolysis and condensation of the APTMS and increases its tendency for homocondensation. The chemical reactivity is thus slowed down, leading to an undesired heterogeneous distribution of functional amino (-NH₂) groups with an insufficient surface coverage of the γ -Fe₂O₃ nanoparticles [50–52].

In contrast to APTMS, under base-catalyzed conditions, the reactivity of tetraethoxysilane (TEOS, Si(OCH₂CH₃)₄) is enhanced due to the number and nature of the alkoxide (i.e., ethoxy) groups, which have a key influence on the crosslinking rate. This higher reactivity of TEOS can be attributed to the inductive stabilization of positively charged intermediates and transition states in the hydrolysis and condensation reactions by the ethoxy groups [53]. Therefore, TEOS was used as a crosslinker and APTMS ((CH₃O)₃-Si-(CH₂)₃-NH₂) was used as a supplier of the -NH₂ functional groups.

In this way, it was possible to create uniform spherical γ -Fe₂O₃@SiO₂-NH₂ core-shell structures with the presence of amino (-NH₂) functional groups on the surface of the nanoparticles, which are required for the subsequent binding of heavy metal ions from water [54].

The adsorption process of heavy metal ions for an adsorbent is highly dependent on the initial pH of the solution, owing to its remarkable effect on the speciation of metal ions [5].

If we take a closer look at the speciation of Cr, Pb, and Hg, we can find that at an acidic pH value, the predominant Cr(VI) species consist of H₂CrO₄⁰, HCrO₄⁻, CrO₄²⁻, and Cr₂O₇²⁻ [5,55] while Cr(III) remains relatively stable in acidic media and is more likely to be oxidized to chromate in alkaline media [56]. For Pb(II) in the pH range from 2 to 6, the dominant form is positively charged Pb²⁺ species, while when the pH values increase above 7, other Pb(II) species—including Pb(OH)⁺, Pb(OH)₂⁰, and PbO—are usually present [57].

Mercury has two common cations in aqueous solutions: a di-ion, Hg₂²⁺, composed of two singly charged ions; and a doubly charged Hg²⁺. Diagrams of Eh-pH indicate that Hg(I) is stable only within a narrow band of Eh values in acidic solutions, while Hg(II) is the dominant form of the Hg species in most aqueous solutions [58]. The hydrolysis reactions of Hg(II) are significant at pH > 1, and different hydrolyzed forms can be formed depending on the aqueous mercury concentration [59]. At low aqueous mercury concentrations, the dominant hydrolysis species formed are HgOH⁺ and Hg(OH)_{2(aq)}, while at higher mercury concentrations the formation of Hg₂(OH)₂²⁺ and Hg(OH)₃⁻ at pH > 13 has been reported [60].

Insoluble metal species will usually not form at pH < 7.2 as long as their concentration is below the solubility limit [61–63]. Therefore, at acidic pH values, the removal of positive heavy metal ions is mainly accomplished by adsorption. In contrast, at higher solution pH values, the precipitation of metal hydroxides or even oxides (e.g., Pb(OH)₂, PbO, CrO₄²⁻,

etc.) can occur as a consequence of the low solubility of metal ions [57]. Therefore, at higher pH values, precipitation of insoluble species may take place at the same time alongside adsorption in the process of heavy metal removal, negatively affecting the adsorption efficiency [64].

Many studies have shown that metal ions start to precipitate as hydroxides or oxides when the solution pH is above 7.2. To avoid precipitation of the metal ions, all adsorption experiments should be conducted at a pH below 7.2 [56,61–63].

Moreover, the adsorption capacity of heavy metal ions decreases with increasing pH values. Specifically, it was shown that the maximum adsorption capacity of Cr(VI) is observed at a pH of 2 [5]. Moreover, the optimal pH for adsorbing Pb(II) was shown to be around 5.5 [65], whereas it was about 6 for Fe₃O₄@SiO₂-NH₂ magnetic nanoparticles [54,61].

Furthermore, it is generally known that iron oxides (γ-Fe₂O₃, Fe₃O₄, etc.) suffer from a tendency to aggregate and decompose in acid-regenerated solutions; thus, to avoid the risk of potential dissolution of iron oxide cores at low pH, in this study, we instead used them in adsorption processes at pH > 3, despite silica shell protection (γ-Fe₂O₃@SiO₂-NH₂) [61].

Iron oxide nanoparticles—i.e., goethite (α-FeOOH), hematite (α-Fe₂O₃), magnetite (Fe₃O₄), maghemite (γ-Fe₂O₃) [66–70],—show moderate affinity towards HM ions on their surface. They appear more applicable if the surface is stabilized [71–73], and enlarged by coating with silica NPs (-SiO₂), whereby agglomeration is prevented [74]. Additionally, by using different functional groups [71–73]—e.g., amino (-NH₂) [34,66–68,75,76], mercapto (-SH) [77,78], carboxy (-COOH) [79]—the adsorption efficiency and adsorption capacity of HM ions can be improved [33,34,71].

Adsorption studies of HM ions from model water by various magnetic nanoparticles (MNPs) and functionalized magnetic nanoparticles (F-MNPs) show that the maximum adsorption capacity of specific HM ions—i.e., for lead [44,61], mercury [80], and chromium [5,81]—can be obtained in less acidic pH.

In Tables 1–3, the adsorption capacity and desorption efficiency are compared for the tested MNPs and amino-functionalized MNPs at the optimal model solution pH values for adsorbing individual HM ions (e.g., Pb²⁺, CrT/Cr³⁺/Cr⁶⁺, and Hg²⁺).

Table 1 shows comparison of the adsorption capacities and desorption efficiency for Pb²⁺ ions by non-functionalized and functionalized MNPs. It can be seen that the adsorption of Pb²⁺ ions was tested mostly at acidic pH, and that the adsorption capacity is higher for the cases of functionalized magnetic nanomaterials. Ahmadi et al. (2014) [35] prepared γ-Fe₂O₃ NPs via the wet chemical method and tested adsorption at pH 7.5, while Nicola et al. (2020) [82] synthesized Fe₃O₄@SiO₂ NPs and found that the adsorption capacity on non-functionalized MNPs was relatively low at pH 6.0 (10.55 mg/g) but a shade higher (14.9 mg/g) for SiO₂-stabilized magnetic nanomaterials [82]. Nicola et al. (2020) [82] also tested the desorption efficiency of Pb²⁺ ions with 5% HCl, and the final desorption efficiency was evaluated as 95.7% [82]. Qian et al. (2019) [36] stated that the adsorption capacity of materials functionalized with chitosan and with an amino group (NH₂-functionalized Fe₂O₃/chitosan NPs) at pH 5.0 was not significantly better compared to NH₂-functionalized Fe₂O₃ materials. Higher adsorption capacity with Fe₃O₄ NPs coated with activated carbon was achieved at pH 6.0 [83], while Huang et al. (2020) [5] reached 53.9 mg/g with amino-functionalized graphene oxide at pH 5.0. Wang et al. (2010) [43] and Tang et al. (2013) [34] stated that even higher adsorption capacity at pH 6.2 (76.66 mg/g) can be achieved by pre-stabilization with SiO₂ and amino-functionalization of magnetic materials (Fe₃O₄@SiO₂-NH₂ NPs). Tang et al. (2013) [34] achieved 82.29 mg/g with amino-functionalized Fe₃O₄@mesoporous SiO₂ core-shell composite microspheres at pH 5.5. In polyethylenimine (PEI)-functionalized Fe₃O₄ magnetic nanoparticles (MNPs) (pH 5.0), adsorption capacity of 60.98 mg/g for Pb²⁺ ions was reported [84]. A maximum adsorption capacity of 60 mg/g at pH 5.0 was achieved using composite beads of *Zea mays* rachis (ZMR) and sodium alginate (AL) as adsorbents [85]. Luo et al. (2021) [86] reported the adsorption of 28.7 mg/g by carbon-doped TiO₂ (C-TiO₂) at pH 6.5 for the adsorption of Pb²⁺. The comparison of adsorption capacities showed that the adsorption capacity of Pb²⁺

ions depends on the pH of the medium, stabilization, and, to a large extent, the presence of $-NH_2$ groups.

Table 1. Comparison of adsorption capacity and desorption efficiency for tested MNPs and amino-functionalized MNPs at the optimal model solution pH for adsorbing Pb^{2+} ions.

Adsorbent	HM Ions	Tested pH	Adsorption Capacity	Desorption Efficiency	Reference
γ -Fe ₂ O ₃ NPs		7.5	10.55 mg/g	-	[35]
Fe ₃ O ₄ @SiO ₂ NPs		6.0	14.9 mg/g	95.7%	[82]
NH ₂ -functionalized Fe ₂ O ₃ /chitosan NPs		5.0	32.46 mg/g	-	[36]
NH ₂ -functionalized Fe ₂ O ₃ NPs		5.0	39.30 mg/g	-	[36]
Magnetic composite of activated carbon and superparamagnetic Fe ₃ O ₄ NPs (Fe ₃ O ₄ @C magnetic composite)		6.0	41.7 mg/g	>77%	[83]
NH₂-functionalized γ-Fe₂O₃ NPs (γ-Fe₂O₃@NH₂ NPs)		4.0	53.5 mg/g	90.7%	This work
Amino-functionalized graphene oxide (GO-NH ₂)	Pb ²⁺	5.0	53.9 mg/g	-	[4]
Fe ₃ O ₄ @SiO ₂ -NH ₂ NPs		6.2	0.37 mmol/g 76.66 mg/g*	-	[43]
Amino-functionalized Fe ₃ O ₄ @mesoporous SiO ₂ core-shell composite microspheres		5.5	82.29 mg/g	-	[35]
NH₂-functionalized γ-Fe₂O₃ NPs (γ-Fe₂O₃@NH₂ NPs)		7.0	83.6 mg/g	91.3%	This work
Polyethylenimine (PEI)-functionalized Fe ₃ O ₄ magnetic nanoparticles (MNPs)		pH 5.0	60.98 mg/g		[84]
Composite beads of <i>Zea mays</i> rachis (ZMR) and sodium alginate (AL)		pH 5.0	60 mg/g		[85]
Carbon-doped TiO ₂ (C-TiO ₂)		pH 6.5	28.7 mg/g		[86]

* calculated.

From the literature, it can be observed that higher adsorption of Cr³⁺/Cr⁶⁺/CrT ions was achieved using amino (-NH₂)-functionalized MNPs (Table 2). The highest adsorption of Cr³⁺ ions by bare MNPs was reported in the literature [72,87,88]. Zhang et al. (2020) [11] used bare magnetic magnetite NPs (Fe₃O₄) for the adsorption of Cr³⁺ ions at pH 4.0 and achieved an adsorption capacity of 8.67 mg/g. Additionally, in acidic media (pH 2.5), Gallo-Cordova et al. (2019) [72] performed adsorption of Cr³⁺ ions using bare iron oxide magnetic NPs and reported an adsorption capacity of 15.0 mg/g, while Hu et al. (2005) [17] achieved a very low adsorption capacity of 19.2 mg/g using maghemite NPs (γ -Fe₂O₃). Zhang et al. (2020) [11], Gallo-Cordova et al. (2019) [72], and Hu et al. (2005) [17] also performed desorption with NaOH, achieving desorption efficiency of >75%, \cong 100%, and 87.7%, respectively. Other studies used amino-functionalized MNPs and achieved higher adsorption capacity in acidic media (pH 2.0 to 3.0). Adsorption of Cr³⁺ ions at pH 3.0 was performed using amino-functionalized magnetite NPs (NH₂-Fe₃O₄) [89]. Baghani et al. (2016) [89] achieved an adsorption capacity of 24.25 mg/g and desorption efficiency of 98.02%. Even better adsorption (i.e., 35.0 mg/g) was reported by Gallo-Cordova et al. (2019) [72] using APTES@TEOS@MNP at pH 2.5, and the desorption efficiency was also high (\cong 100%). Zhao et al. (2010) [44] prepared NH₂-functionalized nanomagnetic polymer adsorbents. Functionalization was performed with different precursors (i.e., EDA-, DETA-, TETA-, TEPA-). A maximum adsorption capacity of 38.5 mg/g at pH 2.5 was achieved using TETA-functionalized nanomagnetic polymer adsorbents. In another study, 40.0 mg/g of Cr³⁺ ions was adsorbed at pH 2.0 by TEPA-functionalized nanomagnetic polymer adsorbents [64]. Huang et al. (2020) [5] reported the adsorption properties of functionalized non-magnetic materials at pH 2.0. Using amino-functionalized graphene oxide (GO-NH₂), Huang et al. (2020) [5] achieved 90.4 mg/g, which is the same adsorption capacity that we achieved with NH₂-functionalized γ -Fe₂O₃ NPs (γ -Fe₂O₃@NH₂ NPs), but at alkaline pH (7.0). The maximum adsorption capacity for chromium(VI) ions was 76.92 mg/g at pH 3.0 when adsorbent carbon-encapsulated hematite nanocubes (α -Fe₂O₃@C) were

used [90]. Puzskarewicz and Kaleta (2019) [91] used activated carbon as an adsorbent, and the maximum adsorption capacity for chromium(VI) ions was 4.35 mg/g at pH 2 [91].

Table 2. Comparison of adsorption capacity and desorption efficiency for tested MNPs and amino-functionalized MNPs at optimal model solution pH for adsorbing CrT/Cr³⁺/Cr⁶⁺/Cr(VI) ions.

Adsorbent	HM Ions	Tested pH	Adsorption Capacity	Desorption Efficiency	Reference
Magnetic magnetite NPs (Fe ₃ O ₄)	CrT/Cr ³⁺ /Cr ⁶⁺ /Cr(VI)	4.0	8.67 mg/g	>75%	[87]
Iron oxide magnetic NPs (MNPs)		2.5	15.0 mg/g	≈100%	[72]
Maghemite NPs (γ-Fe ₂ O ₃)		2.5	19.2 mg/g	87.7%	[88]
NH₂-functionalized γ-Fe₂O₃ NPs (γ-Fe₂O₃@NH₂ NPs)		4.0	24.0 mg/g	-	This work
Amino-functionalized magnetite NPs (NH ₂ -Fe ₃ O ₄)		3.0	24.25 mg/g	98.02%	[89]
APTES@TEOS@MNP		2.5	35.0 mg/g	≈100%	[72]
NH ₂ -functionalized nanomagnetic polymer adsorbents (EDA-NMPs)		2.5	37.6 mg/g	-	[44]
NH ₂ -functionalized nanomagnetic polymer adsorbents (DETA-NMPs)		2.5	37.9 mg/g	-	[44]
NH ₂ -functionalized nanomagnetic polymer adsorbents (TETA-NMPs)		2.5	38.5 mg/g	-	[44]
NH ₂ -functionalized nanomagnetic polymer adsorbents (TEPA-NMPs)		2.0	40.0 mg/g	-	[44]
Amino-functionalized graphene oxide (GO-NH ₂)		2.0	90.4 mg/g	-	[4]
NH₂-functionalized γ-Fe₂O₃ NPs (γ-Fe₂O₃@NH₂ NPs)		7.0	90.4 mg/g	96.7%	This work
Carbon-encapsulated hematite nanocubes (αFe ₂ O ₃ @C)		pH 3	76.92 mg/g		[90]
Activated carbons		pH 2	4.35 mg/g		[91]

The maximum adsorption capacity for Hg²⁺ (Table 3) was 32.88 mg/g at pH 5.0 using carboxyl-terminated hyperbranched poly(amidoamine) dendrimers grafted onto superparamagnetic NPs (CT-HPMNPs) as adsorbents, and the maximum desorption efficiency was ≈85% (using HNO₃ acid) [92]. Wang et al. (2013) [93] used rhodamine-hydrazide-modified Fe₃O₄ as an adsorbent, and the maximum adsorption capacity for Hg²⁺ was 37.4 mg/g at pH 7.5 [93]. Bolivar et al. (2018) [80] performed a study of Hg²⁺ ion adsorption, in which Fe₃O₄ nanoparticles coated with amino organic ligands and yam peel biomass displayed a maximum Hg²⁺ adsorption capacity of 60 mg/g at pH 7.0 [94]. The maximum adsorption capacity for Hg²⁺ was 50 mg/g at pH 7.0 when an adsorbent nanocomposite based on Fe₃O₄ nanoparticles, chitosan nanoparticles, and polythiophene was used [95]. Dun Chen et al. (2016) [96] studied the adsorption of Hg²⁺ using magnetic adsorbents (Fe₃O₄@SiO₂-NH-HCGs; HCG = py (2-pyridinyl); pyd (3-pyridazinyl)) formed by grafting of different heterocyclic groups onto amino groups via substitution reaction. The maximum adsorption capacity for Fe₃O₄@SiO₂-NH-HCG- (pyd) and Fe₃O₄@SiO₂-NH-HCG- (py) was 77 mg/g and 56 mg/g at pH 7.0 [96], respectively. For both adsorption materials, HCl was used as the desorption eluent, and the stated desorption efficiency was 95% [96]. Hao et al. (2021) [97] performed a study of Hg²⁺ ion adsorption with *Armeniaca sibirica* shell activated carbon (ASSAC) magnetized by nanoparticles (Fe₃O₄/ASSAC), showing a maximum adsorption capacity of 97.1 mg/g at pH 2. At pH 5.5, Zhang et al. (2016) [98] studied the adsorption of Hg²⁺ ions with activated carbon (XLAC) derived from *Xanthoceras sorbifolia* Bunge hull as an adsorbent, showing a maximum adsorption capacity of 235.6 mg·g⁻¹. A maximum adsorption capacity of 162 mg g⁻¹ for Hg²⁺ ions at pH 5.0 was achieved using cadmium sulfide nanoparticles doped in a nano-adsorbent fabricated from polycaprolactam (nylon 6) nanofibers (CdS/N6) [99].

Table 3. Comparison of adsorption capacity and desorption efficiency for tested MNPs and amino-functionalized MNPs at optimal model solution pH for adsorbing Hg²⁺ ions.

Adsorbent	HM Ions	Tested pH	Adsorption Capacity	Desorption Efficiency	Reference
NH ₂ -functionalized γ -Fe ₂ O ₃ NPs (γ -Fe ₂ O ₃ @NH ₂ NPs)	Hg ²⁺	4.0	16.2 mg/g	100%	This work
CT-HPMNPs		5.0	32.88 mg/g	≈85%	[92]
Rhodamine-hydrazide-modified Fe ₃ O ₄		7.5	37.4 mg/g	-	[93]
Nanocomposite based on Fe ₃ O ₄ nanoparticles, chitosan nanoparticles, and polythiophene		7.0	50 mg/g	-	[95]
Fe ₃ O ₄ @SiO ₂ -NH-HCG- (py)		7.0	56 mg/g	95%	[96]
Fe ₃ O ₄ nanoparticle coated with amino organic ligands and yam peel biomass		7.0	60 mg/g	-	[94]
Fe ₃ O ₄ @SiO ₂ -NH-HCG- (pyd)		7.0	77 mg/g	95%	[96]
NH ₂ -functionalized γ -Fe ₂ O ₃ NPs (γ -Fe ₂ O ₃ @NH ₂ NPs)		7.0	85.6 mg/g	100%	This work
<i>Armeniaca sibirica</i> shell activated carbon (ASSAC) magnetized by nanoparticles (Fe ₃ O ₄ /ASSAC)		pH 2	97.1 mg/g		[97]
Activated carbon (XLAC) derived from <i>Xanthoceras sorbifolia</i> Bunge hull		pH 5.5	235.6 mg·g		[98]
Cadmium sulfide nanoparticles doped in a nanoadsorbent fabricated from polycaprolactam (nylon 6) nanofibers (CdS/N6)	pH 5	162 mg g		[99]	

Adsorption has predominantly been investigated using -NH₂ [36], -SiO₂ [82], and -SH [94]-functionalized Fe₃O₄ or γ -Fe₂O₃ NPs [67] prepared by different approaches, in model water media of various pH values [34,66], from pH 2.0 to 8.0.

There are not many previous studies [32,66] on testing adsorption by γ -Fe₂O₃ NPs functionalized with an amino (-NH₂) group—specifically, by (3-aminopropyl)trimethoxysilane (APTMS) precursors—and to the best of our knowledge, far less research has been conducted on desorption approaches to date.

Although iron oxide and hybrid iron oxide NPs can be removed from aqueous solutions with an outer magnet, their recycling and regeneration possibilities after adsorption have not been sufficiently explored to fill gaps in the circular economy [32,47,87].

Due to these facts, our challenge was to synthesize and investigate the potential of amino-functionalized γ -Fe₂O₃ MNPs (γ -Fe₂O₃@NH₂ NPs), which would allow efficient adsorption and recycling of HM ions at the shock load concentrations present in the model water, preferably at neutral pH, without pretreatment. To compare adsorption efficiencies and capacities, we tested significant concentrations of Pb²⁺, CrT, and Hg²⁺ ions using different amounts ($m_{ads} = 20/45/90$ mg) of the γ -Fe₂O₃@NH₂ adsorbent NPs at two different pH values of the initial aqueous solution, i.e., at pH = 7.0, as well as at pH = 4.0. Furthermore, before the performance of adsorption tests, -NH₂-functionalized γ -Fe₂O₃ MNPs were characterized with different methods, such as FTIR, BET, TEM, and TGA. Zeta potential changes in γ -Fe₂O₃@NH₂ NPs were analyzed to understand the mechanisms taking place during the adsorption and desorption process of Pb²⁺ ions. Moreover, to evaluate the adsorbent regeneration, desorption with 0.1 M HNO₃ was tested, which is of great importance for the reuse of adsorption materials and recycling of heavy metals. The prepared γ -Fe₂O₃ and functionalized γ -Fe₂O₃@NH₂ MNPs were also characterized by X-ray powder diffractometry (XRD).

2. Results and Discussion

2.1. Properties of the Prepared γ -Fe₂O₃@NH₂ NPs

This section explains the characterization of the synthesized, stabilized, and functionalized MNPs (γ -Fe₂O₃@NH₂ NPs). In addition, the adsorption mechanisms and the results of batch adsorption and desorption experiments are also discussed.

2.1.1. Crystallographic Properties

The prepared γ -Fe₂O₃ and functionalized γ -Fe₂O₃@NH₂ MNPs were characterized by X-ray powder diffractometry (XRD) (Figure 1). In the X-ray powder diffraction pattern in Figure 1, the presence of diffraction peaks at 2θ of 30.2°, 35.5°, 43.2°, 53.6°, 57.2°, and 62.9°—which correspond to the cubic crystal planes of (220), (311), (400), (422), (511), and (440), respectively—are characteristic of the spinel crystal structure (JPCD Card 39-1346). The spinel crystal structure is evident for both samples— γ -Fe₂O₃ and functionalized γ -Fe₂O₃@NH₂ MNPs—while the presence of a broad amorphous diffraction peak for the functionalized γ -Fe₂O₃@NH₂ MNPs, which appears at a low diffraction angle 2θ of 20°, is due to the presence of the amorphous SiO₂ surface layer, indicating that the crystalline cubic spinel γ -Fe₂O₃ magnetic cores were surface-modified [78]. The average size of the γ -Fe₂O₃ crystalline magnetic cores was estimated to be 13 nm, using the Debye–Scherrer equation [100,101].

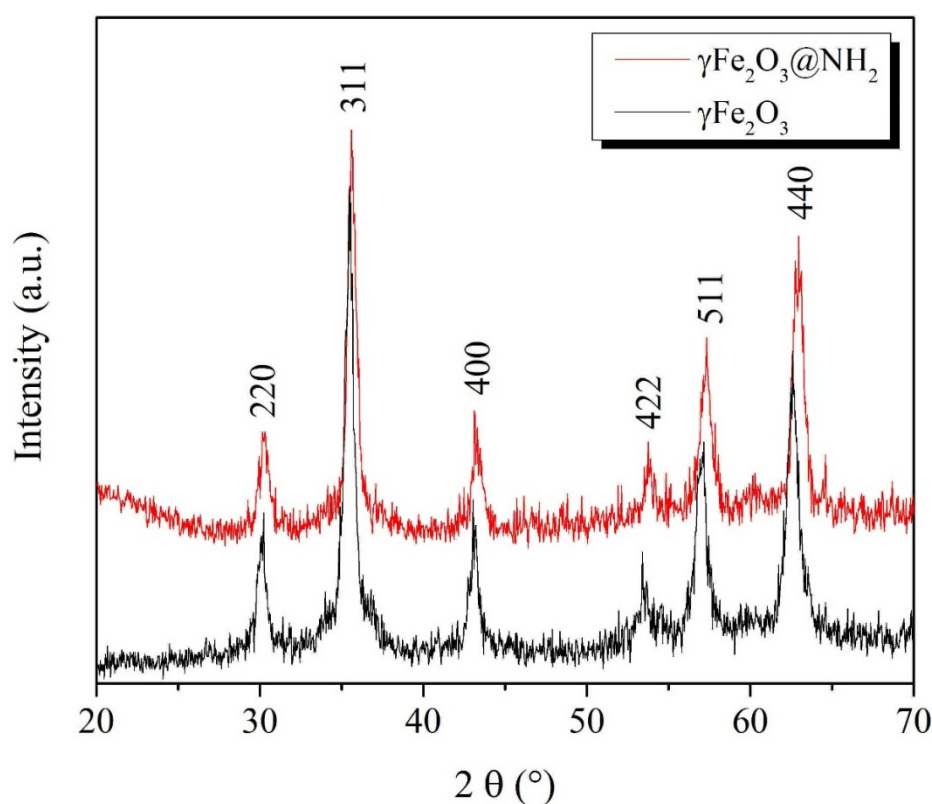


Figure 1. X-ray diffraction patterns (XRD) for the samples γ -Fe₂O₃ and γ -Fe₂O₃@NH₂.

2.1.2. Thermogravimetric Properties

The thermal stability of γ -Fe₂O₃@NH₂ NPs was determined via thermogravimetric analysis (TGA). The results of mass loss during the TGA analysis indicate the possible presence of -NH₂ functional groups on the surface of the F-MNPs. Upon heating up to 180 °C, the measured mass loss corresponds to the evaporation of absorbed moisture and NH₄OH residue. Further weight loss at heating up to 700 °C is due to the removal of aminopropyl (NH₂(CH₂)₃-) groups from the nanoparticles' surfaces and the consequence of cracking of the remaining siloxane groups (Si-O-Si) [75]. The TGA curve (Figure 2) shows that the synthesized, stabilized, and functionalized MNPs have good thermal stability. The weight loss during the TGA analysis was 10.3%.

The thermal stability of the particle samples analyzed was in accordance with previous results in the literature for other functionalized NPs [102–105].

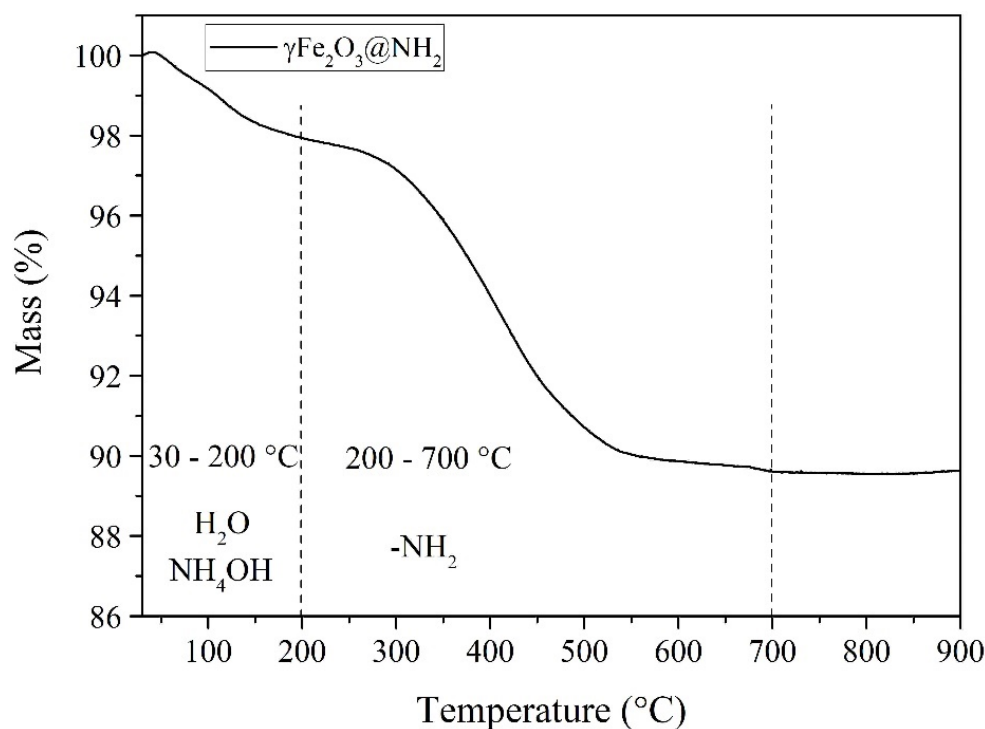


Figure 2. TGA analysis for γ -Fe₂O₃@NH₂ NPs.

2.1.3. FTIR Spectroscopy

An FTIR analysis of γ -Fe₂O₃ and γ -Fe₂O₃@NH₂ NPs was performed comparatively to identify the presence of characteristic functional groups related to the amino-silane coating of the γ -Fe₂O₃ surfaces. The FTIR spectra of γ -Fe₂O₃ and γ -Fe₂O₃@NH₂ NPs, as well as those of pure TEOS and APTMS precursors, are shown in Figure 3a.

The functional amino-silane-coated γ -Fe₂O₃ nanoparticles were derived during the sol-gel process from the mixture of TEOS and APTMS precursors according to the experimental details described in Section 2.4. In contrast to the TEOS precursor (Si(OCH₂CH₃)₄), the APTMS precursor ((CH₃O)₃Si(CH₂)₃NH₂) included a short aliphatic chain (-(CH₂)₃-) and a terminal amino (-NH₂) group in its structure. Thus, the main difference in the FTIR spectra of the TEOS and APTMS precursors is the presence of primary amino (N-H) vibrations in the range of 3400–3300 cm⁻¹ of the APTMS spectra, while both spectra are identical to the occurrence of C-H vibrations in the range of 3000–2800 cm⁻¹ and Si-O-Si vibrations in the range of 1100–1000 cm⁻¹, which are common characteristics of alkoxy-silanes.

As shown in Figure 3a, the formation of the γ -Fe₂O₃ structure is closely related to the occurrence of Fe-O bending and stretching vibrations in the range of 650–550 cm⁻¹. The broad band at 3406 cm⁻¹ observed for the γ -Fe₂O₃ NPs in the wavenumber region 3550–3200 cm⁻¹ can be assigned to intermolecular O-H stretching (Figure 3a).

As opposed to γ -Fe₂O₃ NPs, asymmetric stretching vibrations of Si-O-Si bonds at 1050 cm⁻¹ indicate the formation of a silica (SiO₂) shell in the γ -Fe₂O₃@NH₂ samples. Moreover, two weak bands can be observed for the γ -Fe₂O₃@NH₂ samples in Figure 3a, characteristic of primary amines, due to the asymmetric and symmetric N-H vibrations in the range of 3400–3300 cm⁻¹—more precisely, at 3356 cm⁻¹ and 3281 cm⁻¹, respectively. These primary amino peaks in the source spectra of γ -Fe₂O₃@NH₂ NPs were not sufficiently visible, but enlarged individual peak areas confirmed their presence (Figure 3b). Specifically, the primary amine (NH₂) vibrations occurred in the same wavenumber region as the intermolecular O-H stretching [106]. Because the polarity of the N-H bonds in amines is weaker than that of the O-H bonds, the absorption band of N-H is not as intense as that of O-H, which usually shows stronger and broader absorption bands that are much easier to

identify. Primary amines have also a medium-to-strong absorption band in the wavenumber region $1650\text{--}1580\text{ cm}^{-1}$, which was identified at 1598 cm^{-1} for the $\gamma\text{-Fe}_2\text{O}_3\text{@NH}_2$ NPs [107].

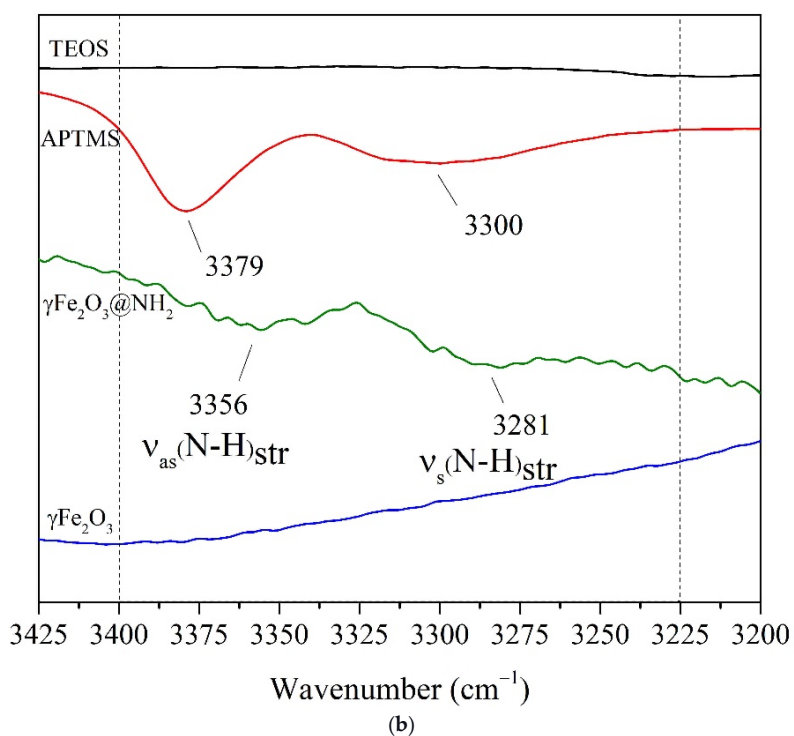
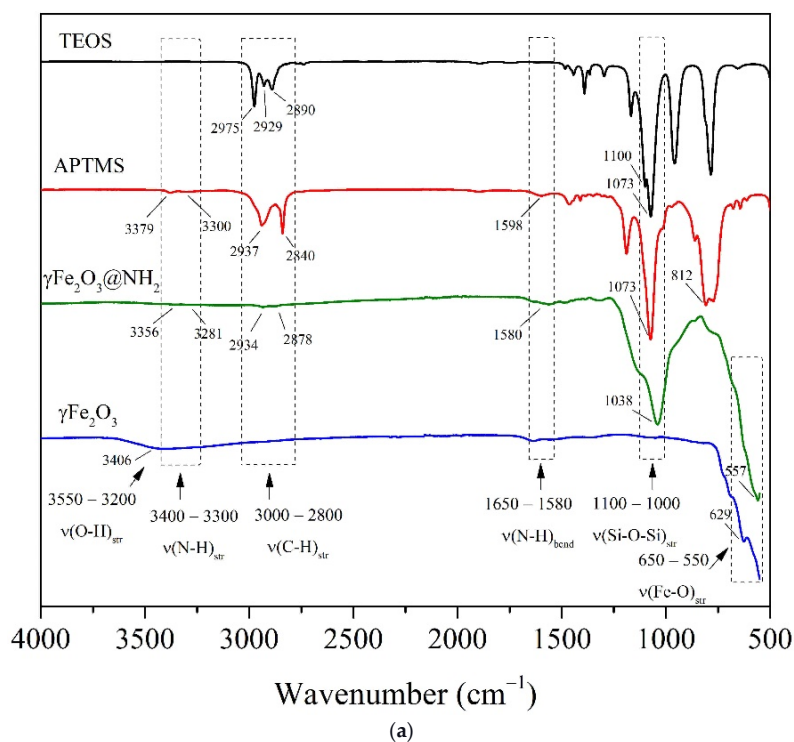


Figure 3. (a) FTIR spectra of $\gamma\text{-Fe}_2\text{O}_3$ NPs, $\gamma\text{-Fe}_2\text{O}_3\text{@NH}_2$ NPs, pure AMPTS precursor, and pure TEOS precursor, and (b) enlarged area corresponding to vibrations of amino (-NH_2) groups.

2.1.4. Specific Surface Area

The specific surface area of the prepared $\gamma\text{-Fe}_2\text{O}_3$ and $\gamma\text{-Fe}_2\text{O}_3\text{@NH}_2$ MNPs was measured by the Brunauer–Emmett–Teller (BET) method. The obtained BET curves are shown in Figure 4.

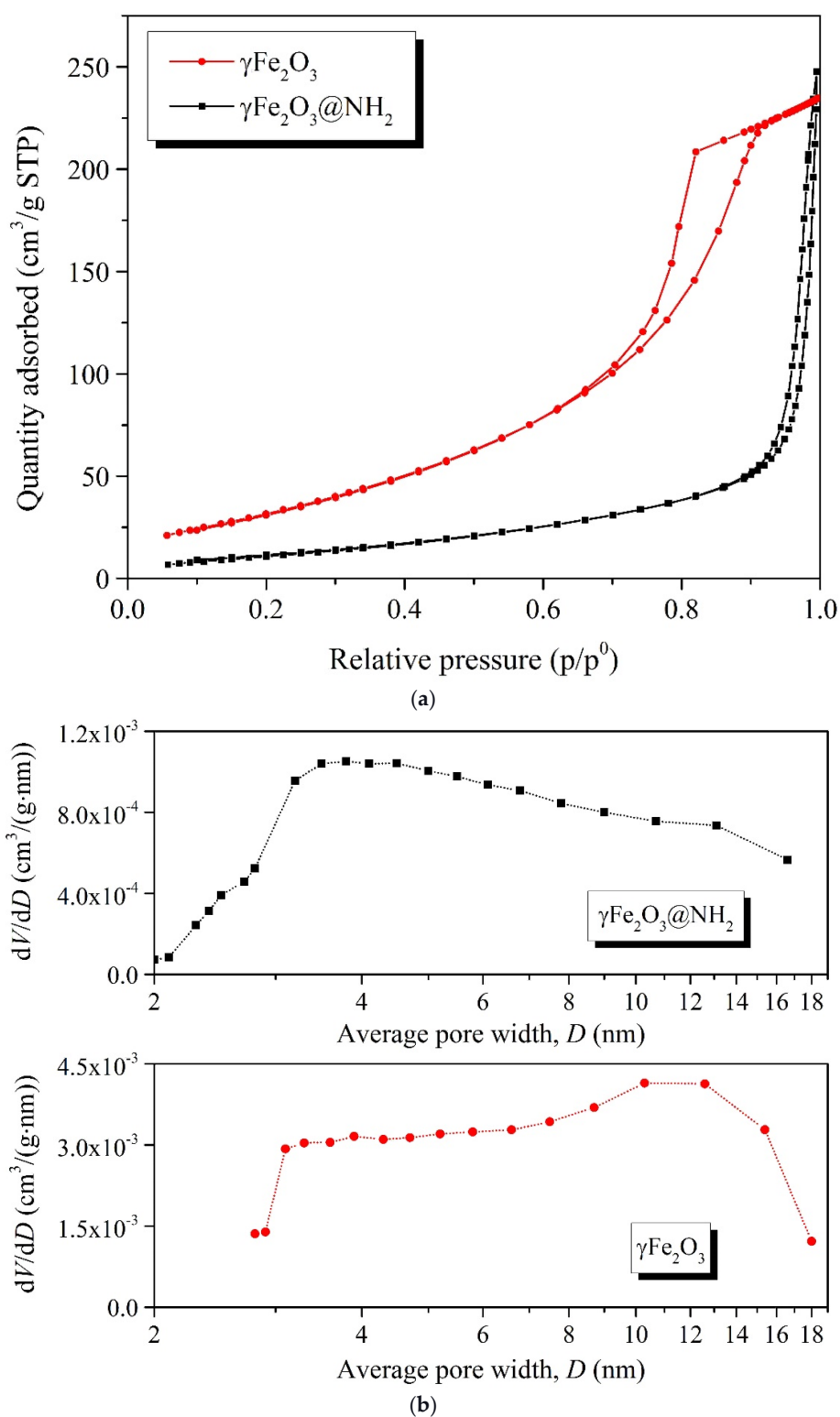


Figure 4. (a) BET isotherms and (b) pore size distribution for $\gamma\text{-Fe}_2\text{O}_3$ and $\gamma\text{-Fe}_2\text{O}_3@\text{NH}_2$ NPs.

The BET analysis showed a specific surface area of 99.9 m²/g for $\gamma\text{-Fe}_2\text{O}_3$ and 41.3 m²/g for $\gamma\text{-Fe}_2\text{O}_3@\text{NH}_2$. According to the Barrett–Joyner–Halenda (BJH) adsorption method, the average pore size was found to be 6.4 nm for the $\gamma\text{-Fe}_2\text{O}_3$ NPs, with a total pore volume of 0.378037 cm³/g, while for the BJH desorption the average pore size for the $\gamma\text{-Fe}_2\text{O}_3$ NPs increased to 6.7 nm, with a total pore volume of 0.407662 cm³/g, suggesting a mesoporous structure of the $\gamma\text{-Fe}_2\text{O}_3$ sample, with a typical type IV experimental N₂ gas

isotherm according to the IUPAC classification [108], as shown in Figure 4. In contrast to $\gamma\text{-Fe}_2\text{O}_3$, the $\gamma\text{-Fe}_2\text{O}_3@\text{NH}_2$ sample showed a BET isotherm with a narrower hysteresis, indicating a decrease in the porosity of the as-prepared $\gamma\text{-Fe}_2\text{O}_3$ sample, most likely due to the presence of the homogeneous silicate coating. For BJH adsorption, the average pore size was found to be 5.8 nm for the $\gamma\text{-Fe}_2\text{O}_3@\text{NH}_2$ NPs, with a total pore volume of $0.090762\text{ cm}^3/\text{g}$, while for the BJH desorption the average pore size for the $\gamma\text{-Fe}_2\text{O}_3@\text{NH}_2$ NPs increased to 6.0 nm, with a total pore volume of $0.090311\text{ cm}^3/\text{g}$.

According to the specific surface area (BET) at a relative pressure (p/p^0) of 0.3, the calculated average particle size was 11.6 nm for $\gamma\text{-Fe}_2\text{O}_3$ and 27.9 nm for $\gamma\text{-Fe}_2\text{O}_3@\text{NH}_2$ NPs [109,110]

2.1.5. Morphological Properties

The results of the TEM analysis (Figure 5a) represent the relatively spherical morphology of the $\gamma\text{-Fe}_2\text{O}_3$ MNPs, with a particle size distribution of $13 \pm 1\text{ nm}$, while the particle size distribution of the functionalized $\gamma\text{-Fe}_2\text{O}_3@\text{NH}_2$ MNPs was $17 \pm 1\text{ nm}$ (magnetic core $13 \pm 1\text{ nm}$ and surface coating $4 \pm 1\text{ nm}$). The electron diffraction pattern of the $\gamma\text{-Fe}_2\text{O}_3$ MNPs inset in Figure 5b indicates the crystalline nature of the as-prepared powders, with concentric diffraction rings characteristic of a cubic spinel crystal structure.

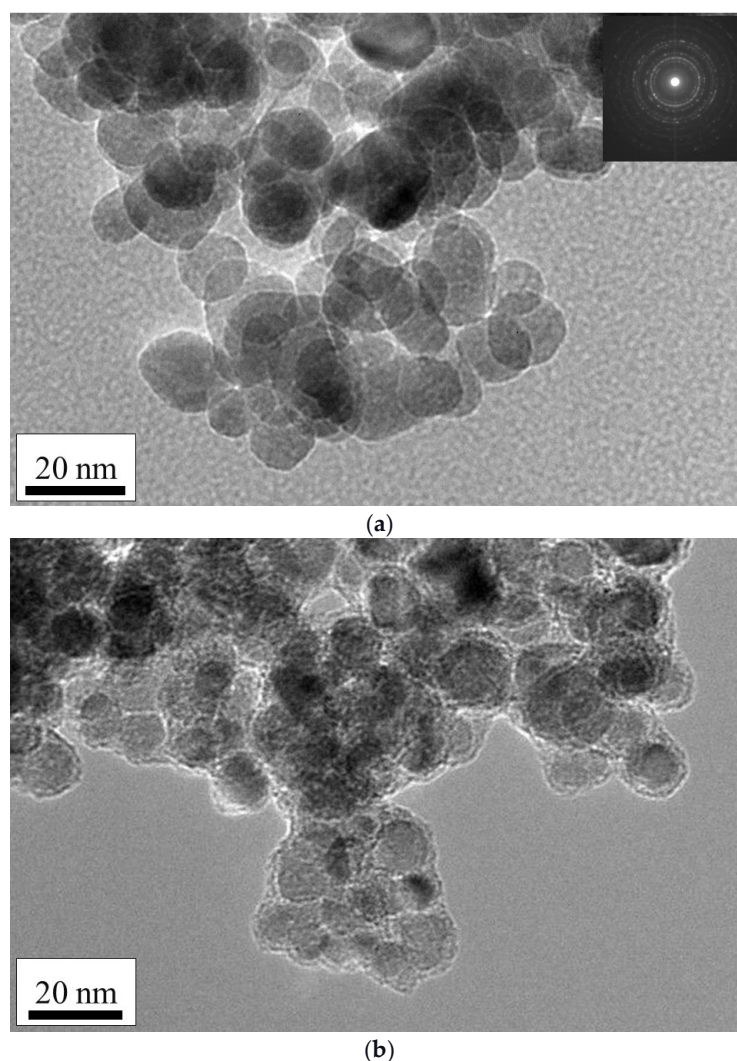
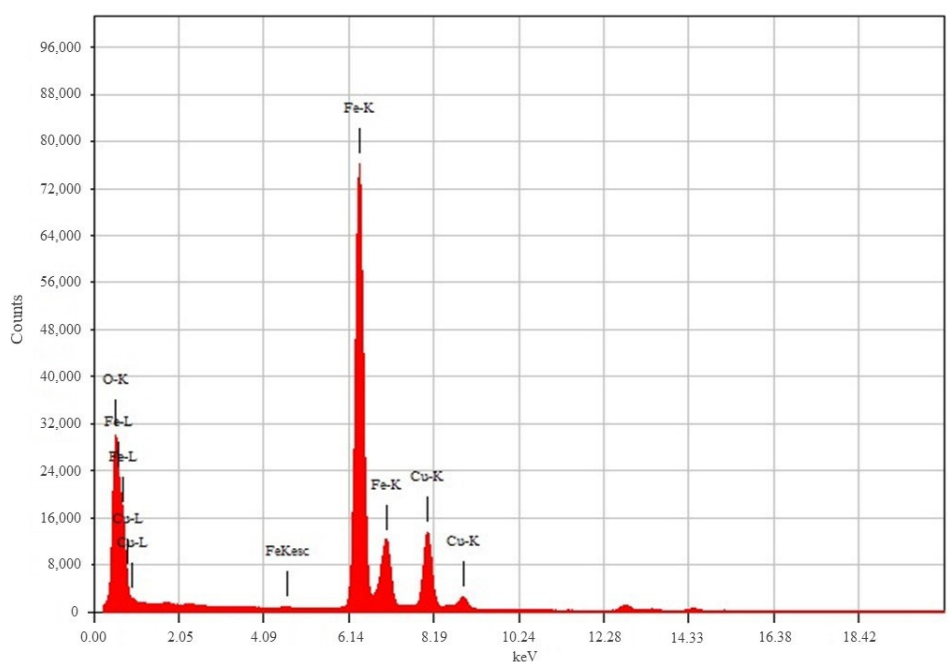
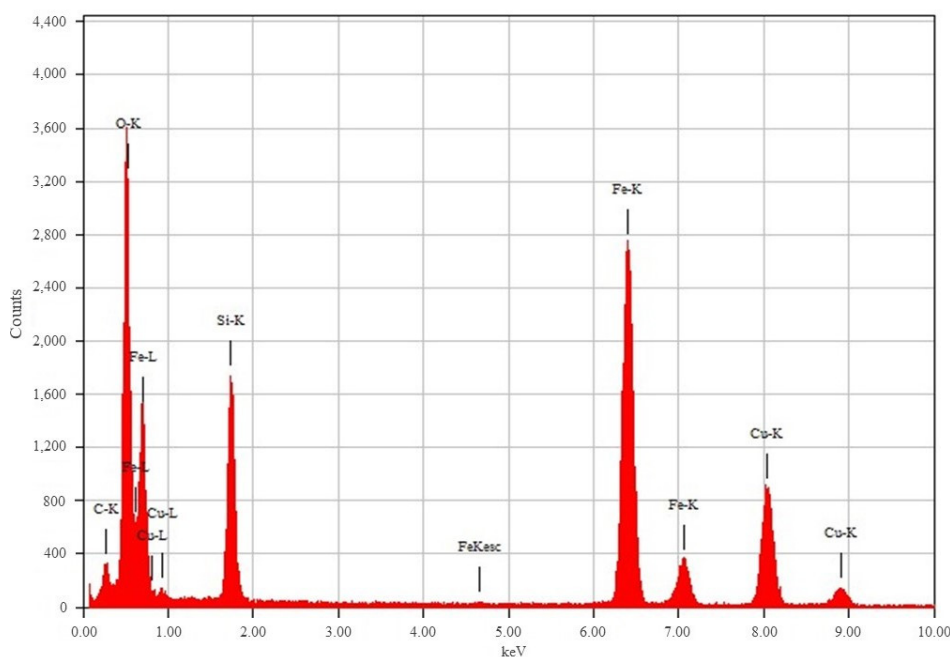


Figure 5. Transmission electron micrographs (TEM) of (a) $\gamma\text{-Fe}_2\text{O}_3$ NPs with inset diffraction pattern and (b) $\gamma\text{-Fe}_2\text{O}_3@\text{NH}_2$ NPs.

The EDXS spectra of the γ -Fe₂O₃ and γ -Fe₂O₃@NH₂ MNPs are shown in Figure 6a,b, respectively. Strong peaks for iron (Fe) and oxygen (O) can be seen in the EDXS spectrum in Figure 6a, indicating the formation of the γ -Fe₂O₃ MNPs. In contrast, the EDXS spectrum of the γ -Fe₂O₃@NH₂ MNPs shows that they contain significant amounts of silicon (Si), alongside iron (Fe) and oxygen (O), suggesting the success of the surface functionalization of γ -Fe₂O₃ MNPs with APTMS precursor molecules and, thus, the formation of the γ -Fe₂O₃@NH₂ MNPs. The lack of a nitrogen (N) peak is expected, due to its low Z-number and overlapping with the K-alpha C and O peaks. The larger peaks towards the right in both EDXS spectra are the copper (Cu) signals sourced from the TEM copper-grid-supported transparent carbon foil.



(a)



(b)

Figure 6. EDXS spectra of (a) γ -Fe₂O₃ NPs and (b) γ -Fe₂O₃@NH₂ NPs.

2.1.6. Zeta Potential

The zeta potential was measured for bare MNPs ($\gamma\text{-Fe}_2\text{O}_3$) and amino-functionalized MNPs ($\gamma\text{-Fe}_2\text{O}_3\text{@NH}_2$), as depicted in Figure 7. For bare, stabilized MNPs, the zeta potential is positive at low pH due to the presence of OH_2^+ . As the pH of the solution increases, the potential decreases and approaches negative potential at high pH, due to the presence of O^- . The measured isoelectric point of the bare MNPs was 8.76 (measured potential -0.743 mV). At this value, the concentration of protonated and deprotonated amino groups is the same. Meanwhile, the measured isoelectric point for functionalized MNPs was at pH 12.1 (measured potential $+0.161$ mV) =, indicating successful MNP functionalization. This difference in the isoelectric point is due to the presence of amino groups on MNPs, resulting in a functionalized magnetic nanomaterial with a negative charge above pH = 12.1.

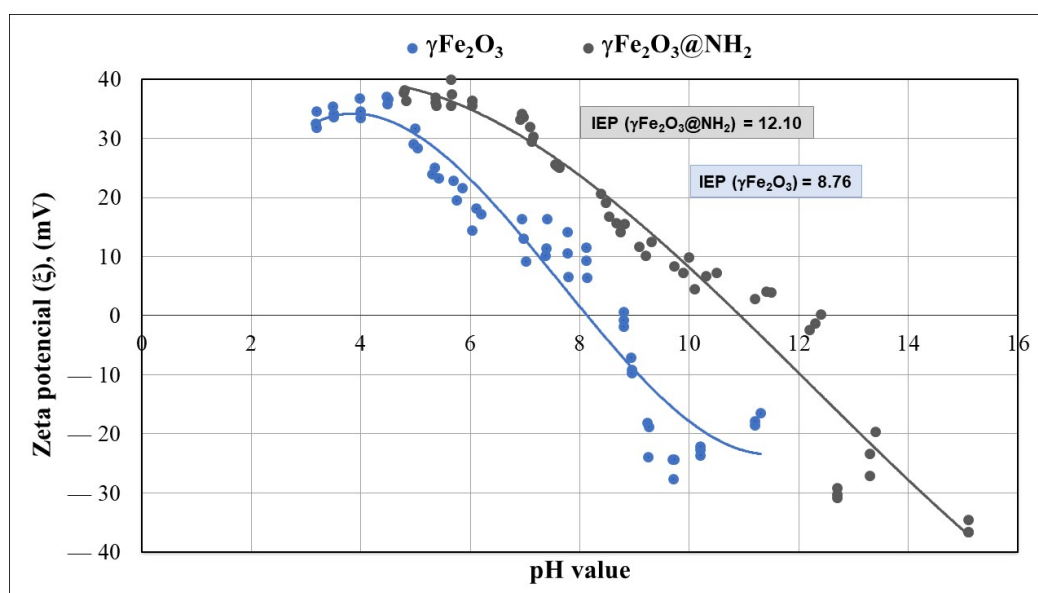


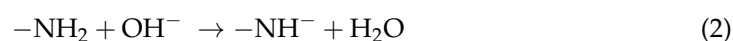
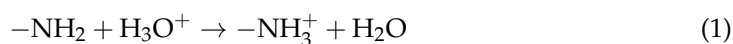
Figure 7. The zeta potential of bare $\gamma\text{-Fe}_2\text{O}_3$ and $\gamma\text{-Fe}_2\text{O}_3\text{@NH}_2$ NPs.

2.2. Adsorption Mechanisms

The solution pH is a key parameter of the effectiveness of HM ions' adsorption. HM ions have specific forms at different pH values; moreover, the adsorbent surface charge and protonation degree of the adsorbent surface coating (i.e., amino groups) are dependent on the pH [111,112]. In general, HM ions' adsorption on $\gamma\text{-Fe}_2\text{O}_3\text{@NH}_2$ NPs includes three sorption mechanisms, i.e., ion exchange, surface complexation, and electrostatic attraction [5]; the specific adsorption mechanism predominantly depends on the solution's pH value [5].

We tested the adsorption of Pb^{2+} , CrT , and Hg^{2+} ions at different pH values, i.e., pH 4 and 7. At different pH values, adsorption takes place by a different mechanism for each metal ion [5].

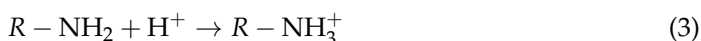
The adsorption of Pb^{2+} ions is entirely dependent on the pH value [70]. The adsorbent surface is negatively charged at alkaline pH, which indicates the deprotonated form of $-\text{NH}_2$ functional groups. The behavior of $-\text{NH}_2$ groups on the adsorbent material according to the pH is shown by Equations (1) and (2) [111]:



At pH 7, $-\text{NH}_2$ groups are deprotonated, causing a negatively charged adsorbent surface, while lead ions are mostly in $\text{Pb}(\text{OH})^+$ form, which causes high electrostatic attraction

between Pb^{2+} ions and the negatively charged material surface and, consequently, high adsorption efficiency [82,111]. On the other hand, acidic conditions cause the transformation of $-\text{NH}_2$ groups into $-\text{NH}_3^+$ form, resulting in fewer available active sites for Pb^{2+} ions. Because of that, the adsorption efficiency of Pb^{2+} ions drops under acidic conditions ($\text{pH} < 7$) [5,111].

The solution pH value is also a key factor in the adsorption efficiency of CrT ions. Adsorption efficiency generally decreases with increasing pH values [5]. In acidic conditions, CrT ions are mainly present as H_2CrO_4^0 , HCrO_4^- , and Cr_2O_7^- species [68,72,81,113], while $-\text{NH}_2$ is present in protonated form, i.e., $-\text{NH}_3^+$ form (Equation (3)). Consequently, the $\gamma\text{-Fe}_2\text{O}_3@-\text{NH}_2$ NPs' surfaces are positively charged [5,81,114]. Strong electrostatic attraction occurs in such cases, and chromium species can be easily captured on the amino-functionalized adsorbent surface [72,81].



On the other hand, at alkaline pH, negatively charged chromate ions (CrO_4^{2-}) are the predominant form [81,87,113]. At $\text{pH} > 7$, $\gamma\text{-Fe}_2\text{O}_3@-\text{NH}_2$ NPs' surfaces are also negatively charged [5] due to the deprotonated form of the amino functional groups. A double-negative charge of the adsorbent surface and chromate decreases the adsorption efficiency [72].

In our study, zeta potential played an important role in the adsorption mechanism. The zeta potential of our $\gamma\text{-Fe}_2\text{O}_3@-\text{NH}_2$ NPs was 8.76; at lower pH, amino groups on the material's surface were mainly present in protonated form ($-\text{NH}_3^+$).

We tested the adsorption of CrT ions at pH 4 and 7. At pH 4, the functional groups were mainly in $-\text{NH}_3^+$ form, while at pH 7 the amino groups were still in protonated form. Consequently, many active sites were present on the surface of the $\gamma\text{-Fe}_2\text{O}_3@-\text{NH}_2$ NPs, so their adsorption capacity was very high. The adsorption efficiency at pH 4 was low due to the instability of $\gamma\text{-Fe}_2\text{O}_3@-\text{NH}_2$ NPs in acidic conditions—the adsorbent material is soluble in acidic media, i.e., at $\text{pH} < 4$.

Hg^{2+} readily reacts with OH^- to form $\text{Hg}_2(\text{OH})_2$ precipitates under alkaline conditions. The adsorption of Hg^{2+} ions is predominantly influenced by the concentration of hydronium ions in aqueous solutions. The change in adsorption at varying pH levels is because the concentration of surface charges governs the adsorbent particles and the degree of ionization of the ions to be removed [111,115,116]. There is a variety of literature suggesting that the adsorption of Hg^{2+} ions favors neutral and basic pH. The rationale for more adsorption of Hg^{2+} ions using amino groups at neutral and basic pH is that the amino group obtains a net positive charge at acidic pH and the Hg^{2+} ions are also positive; hence, the adsorption is made unfavorable by the repulsive force. The above rationale for mercury species in aqueous solution was theoretically determined as a function of pH by modeling chemical equilibrium using MINEQL+ software (Environmental Research Software, Hallowell, ME, USA) [80,117].

2.3. Effects of pH

Batch adsorption experiments of Pb^{2+} , CrT, and Hg^{2+} ions for different adsorption times were performed at two pH values, i.e., pH 4 and 7 (Figures 8–11). The results show that the adsorption of Pb^{2+} and Hg^{2+} ions is more efficient at pH 7. Such results were expected, due to the opposite charges of the Pb^{2+} ions and the surface of the adsorption material. The opposite surface charges caused strong electrostatic interactions and high material uptake.

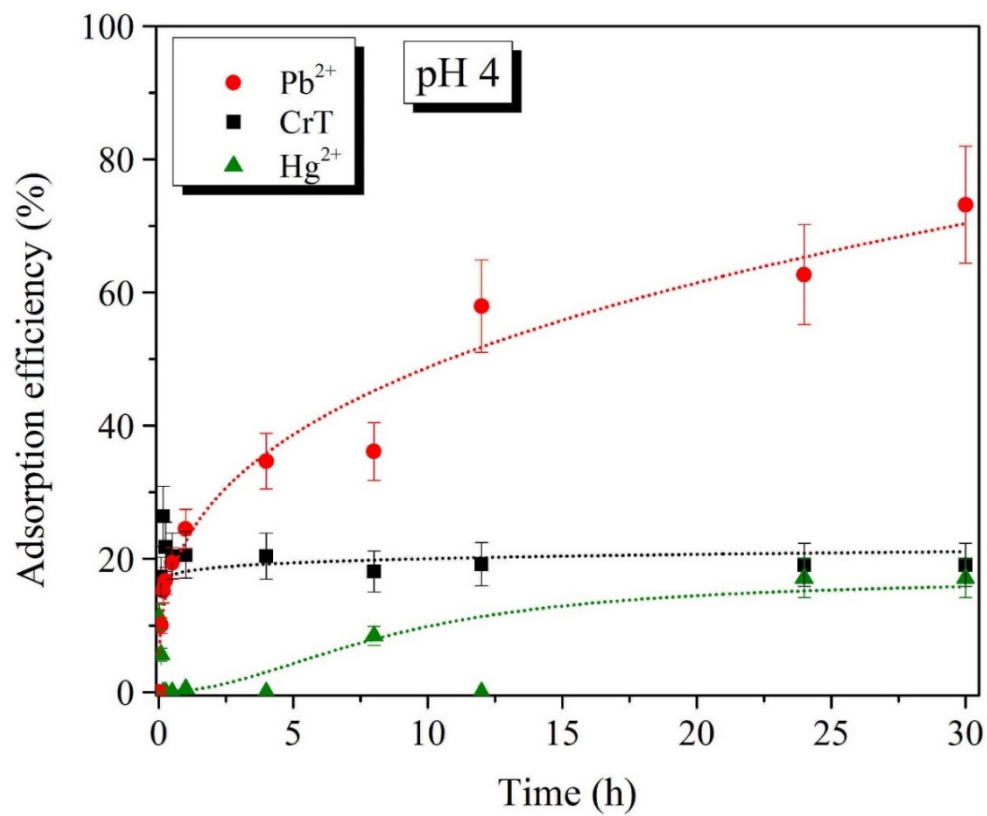


Figure 8. Adsorption efficiency (%) of Pb²⁺, CrT, and Hg²⁺ ions at pH = 4.

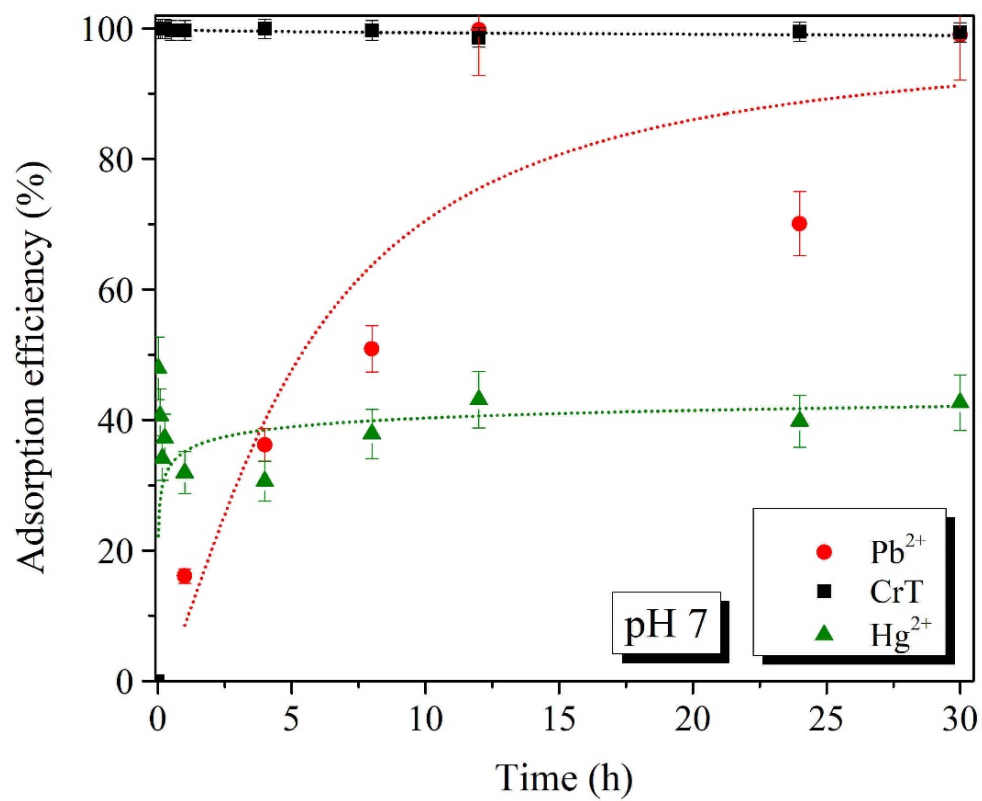


Figure 9. Adsorption efficiency (%) of Pb²⁺, CrT, and Hg²⁺ ions at pH = 7.

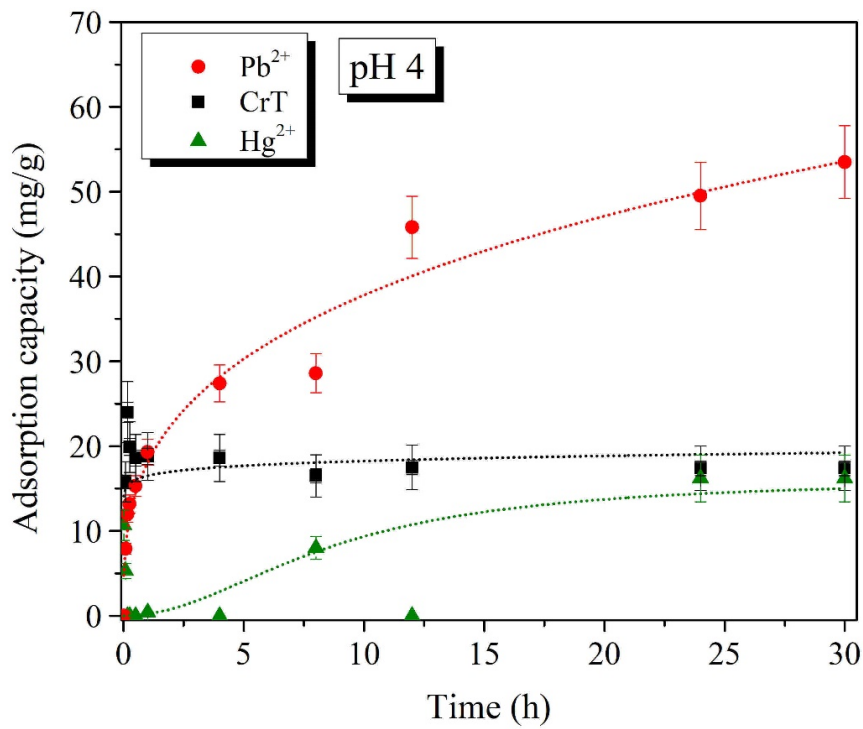


Figure 10. Adsorption capacity (mg/g) of Pb²⁺, CrT, and Hg²⁺ ions at pH = 4.

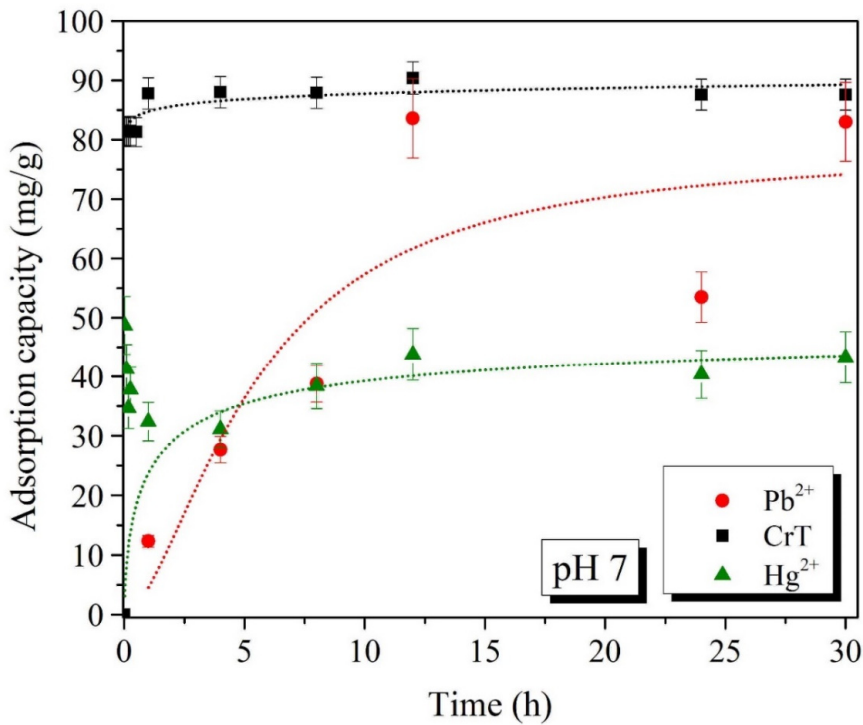


Figure 11. Adsorption capacity (mg/g) of Pb²⁺, CrT, and Hg²⁺ ions at pH = 7.

The adsorption capacity at pH 4 and 7 slowly increased with longer specific adsorption times. At pH 4, the maximal adsorption capacity of Pb²⁺ ions was 53.5 mg/g, which was detected after 30 h. At pH 7, the maximal adsorption capacity of 83.6 mg/g was achieved already after 12 h. At both tested pH values, the adsorption of Pb²⁺ ions slowly increased with a longer adsorption time. This indicates that the adsorption of Pb²⁺ ions is a slow process but, more importantly, the process is efficient—especially at pH 7.

Adsorption of CrT ions was much faster and very efficient at the same time. At pH 4, the adsorption efficiency was lower than 30%, and the maximal adsorption capacity was 24.0 mg/g. γ -Fe₂O₃@NH₂ NPs were less stable in acidic conditions, which was the main reason for the lower material uptake. At pH 7, we achieved 99.9% adsorption efficiency already after 1 min. When the adsorption time was extended, the efficiency stayed high, and the maximal adsorption capacity (90.4 mg/g) was achieved after 12 h.

For Hg²⁺ ions, the maximal adsorption efficiency of 84.3% displayed a corresponding adsorption capacity of 85.6 mg/g, which was reached after 30 min of adsorption time. At pH 4, Hg²⁺ ions showed a low adsorption efficiency of 17%, with a corresponding adsorption capacity of 16.2 mg/g at 30 h. As demonstrated in various studies [80,111,115–117], the increase in pH from 4 to 7 also facilitated the maximal adsorption efficiency.

2.4. Effect of Adsorbent Mass

The adsorption of CrT ions on 45 mg of γ -Fe₂O₃@NH₂ NPs showed excellent results (q_t after 1 min was 81.4 mg/g). To determine the optimal adsorbent mass, we tested different amounts of γ -Fe₂O₃@NH₂ NPs. In adsorption experiments, 20, 45, and 90 mg of γ -Fe₂O₃@NH₂ NPs were investigated under optimal adsorption conditions (pH = 7, $c = 200$ mg CrT/L and RT). Adsorption tests were performed only for 1, 4, 8, 24, and 30 h, as we expected that longer specific adsorption times would be required with smaller amounts of γ -Fe₂O₃@NH₂ NPs.

The results of CrT ions' adsorption showed excellent adsorption efficiency (>99.2%) for all tested amounts of γ -Fe₂O₃@NH₂ NPs at all tested specific adsorption times (Figure 12). The only exception was the test using 20 mg of γ -Fe₂O₃@NH₂ NPs after 1 h. The adsorption efficiency on 20 mg of γ -Fe₂O₃@NH₂ NPs was only 35.3%, indicating insufficient adsorbent mass. Nevertheless, the adsorption efficiency reached 99.9% after 24 h, showing that the adsorption of CrT ions with a smaller amount of γ -Fe₂O₃@NH₂ NPs required a longer adsorption time. Meanwhile, the adsorption of CrT ions on 45 and 90 mg was equal; thus, based on the results of adsorption on 20/45/90 mg of γ -Fe₂O₃@NH₂ NPs, we concluded that 45 mg was the optimal mass of adsorbent.

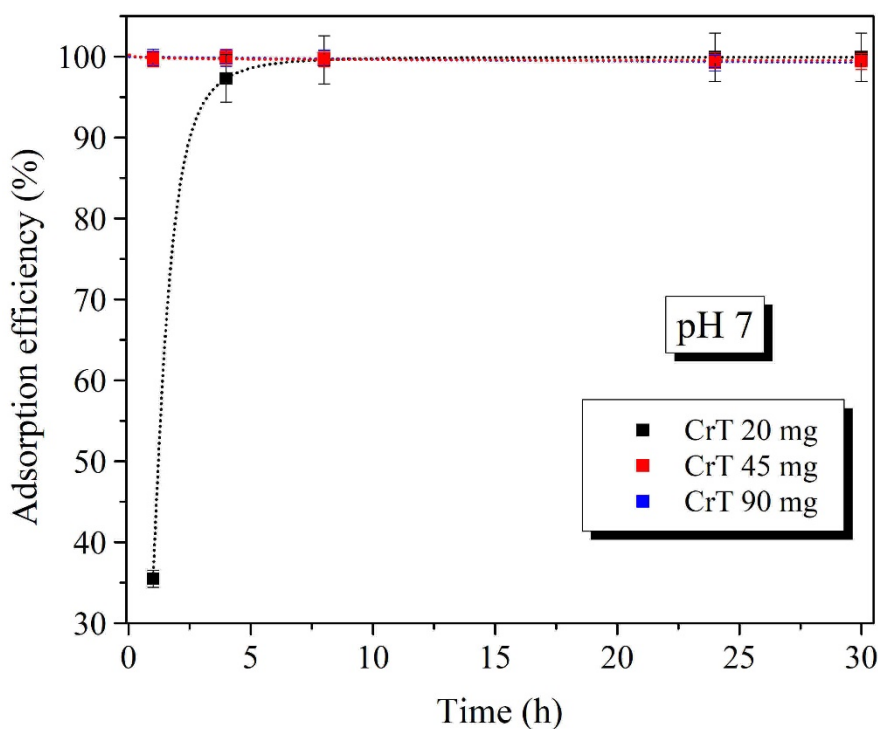


Figure 12. Adsorption efficiency of (%) CrT ions on $m_{\text{ads}} = 20/45/90$ mg pH = 7.

2.5. Effects of Anions (NO_3^- , Cl^- , SO_4^{2-})

The adsorption of CrT ions showed high adsorption efficiency (99.9%) after 1 min. For these reasons, we also tested the impacts of different anions (i.e., NO_3^- , Cl^- , and SO_4^{2-}) on the adsorption efficiency of CrT ions. Experiments were performed under further optimal determined conditions (pH = 7, $m_{\text{ads}} = 45$ mg, $c = 200$ mg CrT/L), and only for 1, 5, 10, 15, 30, 45, and 60 min at RT.

The results showed no effects of different anions; furthermore, the adsorption of CrT ions remained quick, and after 1 min the adsorption efficiency rate was 99.9% for all tested anions (Figure 13).

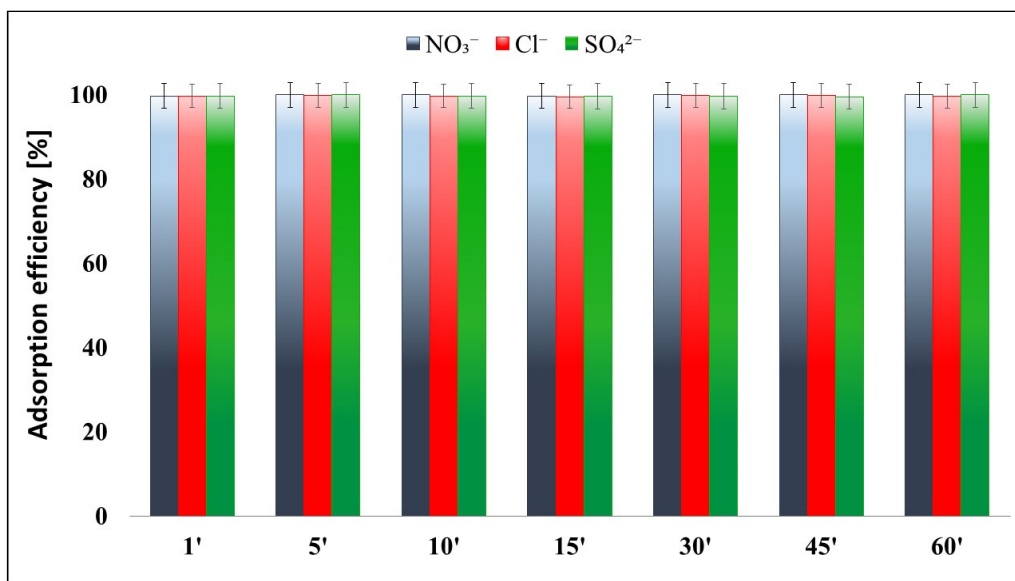


Figure 13. Effects of anions (NO_3^- , Cl^- , and SO_4^{2-}) on the adsorption efficiency (%) of CrT ions pH = 7.

2.6. Desorption

To verify the possibility of recycling HM ions and reusing adsorption materials, desorption of Pb^{2+} , CrT, and Hg^{2+} ions was performed. Due to the higher adsorption capacity of metal ions at 1140 and 1800 min, adsorption was tested for longer specific adsorption times. Desorption was performed in one cycle because of material loss during the desorption process. The results of desorption showed that the $\gamma\text{-Fe}_2\text{O}_3@ \text{NH}_2$ NPs enabled high desorption efficiency for the samples on the surface of which the HM ions' adsorption was performed at pH 7. This result indicates the electrostatic binding of HM ions on the adsorption material's surface. Electrostatic binding of HM ions is weaker than covalent interactions, which probably appear at lower pH, i.e., pH 4. For this reason, only desorption results of samples after adsorption was performed at pH 7 are reported in this work (Figure 14).

The first desorption cycle performed with 0.1 M HNO_3 was more efficient for Hg^{2+} , CrT, and Pb^{2+} ions. For Pb^{2+} ions, the desorption efficiency was 91.3%; for CrT it was 96.7%; and for Hg^{2+} ions it was 100%. From the obtained results, it was possible to determine that higher desorption efficiency was achieved for all tested HM ions with a longer specific adsorption time (i.e., 30 h).

The desorption efficiency of Hg^{2+} ions showed that the $\gamma\text{-Fe}_2\text{O}_3@ \text{NH}_2$ NPs enabled high desorption efficiency (100%) for all samples, with the adsorption process being carried out at pH 4 and 7.

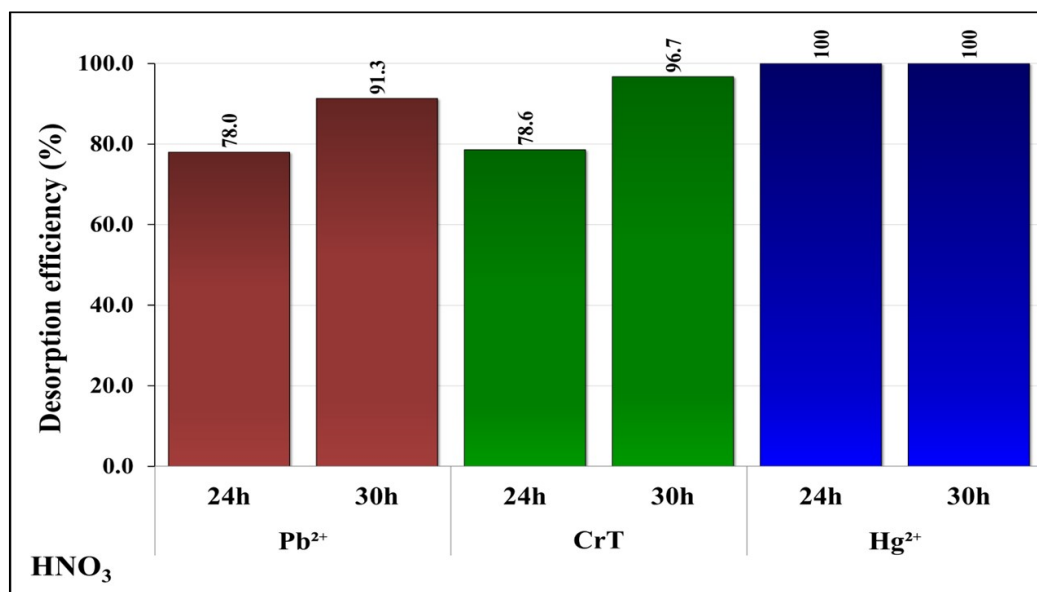


Figure 14. Desorption efficiency of Pb²⁺, CrT, and Hg²⁺ ions (after specific adsorption times at pH = 7). Desorption was performed with 0.1 M HNO₃ for 60 min.

3. Methods and Materials

3.1. Materials

For the lab-scale synthesis, stabilization, and functionalization of γ -Fe₂O₃ MNPs, iron(II) sulfate heptahydrate (FeSO₄ 7H₂O, 99.5%, 278.01 g/mol, CAS 7782-63-0, Honeywell International Inc., Charlotte, NC, USA), iron(III) sulfate hydrate (Fe₂(SO₄)₃ xH₂O, 97%, 399.88 g/mol, CAS 15244-10-7, Honeywell International Inc., Charlotte, NC, USA), tetraethyl orthosilicate TEOS (C₆H₂₀O₄Si, 99%, 208.33 g/mol, CAS 78-10-4, Sigma-Aldrich, Merck Group KGaA, Darmstadt, Germany), (3-aminopropyl)trimethoxysilane APTMS (C₆H₁₇NO₃Si, 97%, 179.29 g/mol, CAS 13822-56-5, Sigma-Aldrich, Merck Group KGaA, Darmstadt, Germany), ammonium hydroxide (NH₄OH, 25%, 35.05 g/mol, CAS 1336-21-6, GramMol, Zagreb, Croatia), ethanol (C₂H₅OH, 96%, 46.07 g/mol, CAS 64-17-5, GramMol, Zagreb, Croatia), and 2-propanol (C₃H₇OH, 99.9%, 60.10 g/mol, CAS 67-63-0, GramMol, Zagreb, Croatia) were used. For the batch adsorption experiments, aqueous solutions were prepared from lead(II) nitrate (Pb(NO₃)₂, 99.9%, 331.21 g/mol, CAS 10099-74-8, Sigma-Aldrich, Merck Group KGaA, Darmstadt, Germany), chromium(III) nitrate nonahydrate (Cr(NO₃)₃ 9H₂O, 99%, 400.15 g/mol, CAS 7789-02-8, Sigma-Aldrich, Merck Group KGaA, Darmstadt, Germany), mercury(II) nitrate monohydrate (Hg(NO₃)₂ H₂O, ≥99.99%, 342.62 g/mol, CAS 7783-34-8, Sigma-Aldrich, Merck Group KGaA, Darmstadt, Germany), chromium(III) chloride hexahydrate (CrCl₃ 6H₂O, ≥98%, 266.45 g/mol, CAS 10060-12-5, Sigma-Aldrich, Merck Group KGaA, Darmstadt, Germany), and chromium(III) sulfate hydrate (Cr₂(SO₄)₃ xH₂O, 99%, 392.17 g/mol, CAS 15244-38-9, Sigma-Aldrich, Merck Group KGaA, Darmstadt, Germany). Chemicals were used as purchased. For the preparation of suspensions and solutions, deionized water (dH₂O) was used.

3.2. Synthesis of MNPs

The synthesis of the maghemite (γ -Fe₂O₃) MNPs was carried out as described in our previous studies [32]. First, 30 mL of NH₄OH was added to a 100 mL glass flask and heated up to 90 °C in an oil bath, under constant stirring at 220 rpm. Afterward, 50 mL of an aqueous solution prepared at a stoichiometric ratio of 1:2 using FeSO₄ 7H₂O and Fe₂(SO₄)₃ xH₂O salts was added to the reaction flask. Synthesis then proceeded in alkaline conditions at pH 10 for 1 h at 90 °C. After the reaction was finished, the suspension was cooled down to room temperature (RT), and the magnetic sediment was settled out for 30 min using an external permanent magnet. After magnetic separation, the supernatant was decanted and

discarded. The colloid was rinsed several times with dH₂O, centrifuged at 3500 rpm for 15 min and, finally, separated and allowed to settle on the external magnet overnight.

3.3. Stabilization of MNPs

The rinsed γ -Fe₂O₃ MNPs were suspended in 100 mL of NH₄OH overnight at RT under constant stirring (330 rpm) for the stabilization process. After 16 h, the stabilized maghemite MNPs were separated into two phases overnight on an external magnet. The upper phase was decanted, and the colloid was prepared for further functionalization.

3.4. Functionalization of MNPs

Amino-functionalization of the γ -Fe₂O₃ MNPs was carried out with tetraethyl orthosilicate (TEOS) and (3-aminopropyl)trimethoxysilane (APTMS) precursors, with a water-to-TEOS molar ratio R = 293 and TEOS-to-APTMS molar ratio P = 1:2. After the stabilization phase, 4 mL of γ -Fe₂O₃ colloidal solution was added to the mixture of 21.6 mol% 2-propanol, 2.2 mol% NH₄OH, 15.1 mol% dH₂O, 0.25 mol% TEOS, and 0.36 mol% APTMS, and then mixed vigorously for 5 min. After 24 h of reaction (at RT under constant stirring at 220 rpm), the colloidal solution was intensively washed with ethanol and dH₂O and centrifuged at 3500 rpm for 5 min to remove agglomerates of non-functionalized γ -Fe₂O₃ MNPs.

3.5. Characterization of Amino-Functionalized γ -Fe₂O₃ MNPs

Characterization of the lab-scale amino-functionalized γ -Fe₂O₃ MNPs (γ -Fe₂O₃@NH₂ NPs) was performed using the appropriate method after each preparation phase (i.e., synthesis, stabilization, functionalization). For characterization purposes, the γ -Fe₂O₃@NH₂ MNPs were dried at 90 °C overnight, and the mass of the obtained dried particles was determined. The prepared γ -Fe₂O₃ and functionalized γ -Fe₂O₃@NH₂ MNPs were characterized by X-ray powder diffractometry (XRD) (Bruker D4 Endeavor, Bruker, Billerica, MA, USA). The thermogravimetric properties were analyzed with a 4000 TGA PerkinElmer analyzer (PerkinElmer, Waltham, MA, USA), FTIR spectra were recorded with a Spectrum Two (PerkinElmer, Waltham, MA, USA), and specific surface area (BET) was measured with a TriStar II 3020 (Micromeritics Instrument Corporation, Norcross, GA, USA). The morphology of the synthesized γ -Fe₂O₃@NH₂ MNPs was investigated using a transmission electron microscope (JEM 2100 JEOL, JEOL Ltd, Musashino Akishima, Tokyo, Japan) equipped with an energy-dispersive X-ray spectroscopy (EDXS) unit and a CCD camera to capture images.

3.6. Adsorption of Heavy Metal Ions in Aqueous Solutions

Batch adsorption tests of Pb²⁺, CrT, and Hg²⁺ ions were performed. The initial concentration of 200 mg/L of HM ions in the model water solutions was prepared by dissolving Pb(NO₃)₂, Cr(NO₃)₃·9H₂O, and Hg(NO₃)₂·H₂O in a 1 L flask. The adsorption efficiency (R %) and adsorption capacity (q_t mg/g) at different pH of the model solution and adsorption at the defined time were calculated using Equations (6) and (7). Additionally, the effect of different adsorbent mass (m_{ads} = 20, 45, 90 mg) was tested, and the impact of various anions (e.g., NO₃⁻, Cl⁻, and SO₄²⁻) on the adsorption of CrT ions was investigated. For Pb²⁺ and Hg²⁺ ions, only adsorption at different pH values was tested.

The initial pH values of the solutions were measured and set to pH 4 with 0.1 M and 1 M HNO₃ to simulate an acidic environment, which does not affect the γ -Fe₂O₃@NH₂ NPs, while 1 M NaOH was used to adjust the pH to 7 to simulate actual wastewater conditions. Adsorption was conducted in 50 mL plastic centrifuges into which 20, 45, or 90 mg of the lab-scale γ -Fe₂O₃@NH₂ NPs were weighed. Then, 20 mL of the prepared model salt solution was added to the γ -Fe₂O₃@NH₂ NPs for selected specific adsorption times (1, 5, 10, 15, 30, 60, 240, 480, 720, 1140, and 1800 min). All tests were carried out at RT. To separate the γ -Fe₂O₃@NH₂ NPs from the supernatant after adsorption, a centrifuge (4500 rpm, 15 min) (UNIVERSAL 320, Andreas Hettich GmbH & Co. KG, Tuttlingen, Germany) and

an external magnet were used. The supernatant was decanted into a glass vial; meanwhile, the $\gamma\text{-Fe}_2\text{O}_3\text{@NH}_2$ NPs were washed two times with 10 mL of dH_2O .

The concentration of the HM ions in the supernatant was measured via atomic adsorption spectroscopy (AAS PerkinElmer, PerkinElmer, Waltham, MA, USA) and inductively coupled plasma optical emission spectrometry (ICP-OES, SPECTRO CITROS VISION, SPECTRO Analytical Instruments GmbH, Kleve, Germany) for Hg^{2+} . For both analyses, the supernatants were acidified with HNO_3 (0.5 mL of acid to 10 mL of the supernatant sample).

The adsorption efficiency (R %) was calculated using Equation (6) [87]:

$$R = \frac{(C_0 - C_t)}{C_0} \times 100 \quad (6)$$

where R (%) is the adsorption efficiency, C_0 (mg/L) is the initial concentration of HM ions, and C_t (mg/L) is the residual concentration of HM ions.

The adsorption capacity was calculated using Equation (7) [87]:

$$q_t = (C_0 - C_t) \times \frac{V}{m} \quad (7)$$

where q_t (mg/g) is the adsorption capacity, C_0 (mg/L) is the initial concentration of HM ions, C_t (mg/L) is the residual concentration of HM ions, V (mL) is the solution volume, and m (mg) is the adsorption material mass.

3.7. Desorption of HM Ions and Regeneration Experiments

The desorption experiments for Pb^{2+} , CrT, and Hg^{2+} ions were conducted to evaluate the recyclability of $\gamma\text{-Fe}_2\text{O}_3\text{@NH}_2$ NPs. Desorption tests were performed immediately after specific adsorption times—i.e., 1, 1140, and 1800 min—and after rinsing twice with 10 mL of distilled water. Desorption was performed at RT with 20 mL of 0.1 M HNO_3 added to 45 mg of adsorbent material. Desorption was in contrast to adsorption performed in dynamic mode with an IKA MS3 digital shaker (IKA-Werke GmbH & Co. KG, Staufen, Germany) at minimal rpm. The desorption efficiency was evaluated with AAS for Pb^{2+} and CrT, and with ICP-OES for Hg^{2+} ions.

4. Conclusions

In this study, stabilized and amino-functionalized magnetic nanoparticles ($\gamma\text{-Fe}_2\text{O}_3\text{@NH}_2$ NPs) with a diameter of 17 ± 1 nm were synthesized, characterized, and used as adsorbents for Pb^{2+} , CrT, and Hg^{2+} ions. Adsorbent characterization showed that $\gamma\text{-Fe}_2\text{O}_3\text{@NH}_2$ NPs have good thermal stability. The particles were successfully stabilized, and amino-functionalization was confirmed with FTIR spectroscopy.

The adsorption process was carried out in aqueous solutions at pH 4 and 7. The adsorption results showed the highest adsorption efficiency and capacity at pH 7 for all investigated heavy metal (HM) ions, i.e., Pb^{2+} , CrT, and Hg^{2+} . The adsorption efficiency was the highest and quickest for $\text{CrT} > \text{Hg}^{2+} > \text{Pb}^{2+}$ ions. The maximal adsorption capacity for Hg^{2+} ions was achieved in 30 min, at 85.6 mg/g; for CrT and Pb^{2+} ions, the maximal adsorption capacities were achieved after 12 h and were 90.4 mg/g and 83.6 mg/g, respectively. Experiments with different amounts of $\gamma\text{-Fe}_2\text{O}_3\text{@NH}_2$ NPs (20/45/90 mg) showed that the optimal mass of adsorbent was 45 mg. Moreover, under optimal adsorption conditions (pH = 7, $m_{\text{ads}} = 45$ mg, $c = 200$ mg CrT/L, and RT), different anions—i.e., NO_3^- , Cl^- , and SO_4^{2-} —showed no effect on the adsorption efficiency of CrT ions.

A study of the desorption process with 0.1 M HNO_3 for 1 h showed the possibility of reusing $\gamma\text{-Fe}_2\text{O}_3\text{@NH}_2$ NPs. Desorption was effective only for $\gamma\text{-Fe}_2\text{O}_3\text{@NH}_2$ NPs after the adsorption process was performed at neutral pH. We observed excellent desorption efficiency for Hg^{2+} (100%), CrT (96.7%), and Pb^{2+} (91.3%) ions.

The adsorption–desorption results showed that $\gamma\text{-Fe}_2\text{O}_3\text{@NH}_2$ NPs have great ability and potential for specific and selective binding of HM ions and show excellent potential

for real application in the circular economy. For this reason, further investigation of the circular adsorption–desorption process for different HM ions (such as copper, iron, and cadmium) in a single or binary system should be carried out in the near future.

The use of functionalized magnetic nanomaterials as adsorbents in this study showed that they combine the advantages of magnetic properties—which allow the removal of pollutants from water using an external magnetic field—with the properties of other functional materials, improving their adsorption, separation, and regeneration properties. Such adsorption materials are capable of removing the main components of inorganic pollutants, such as heavy metal ions, under different concentrations and pH conditions, due to their chemical and physical stability.

At the same time, this study showed that such functional magnetic nanoparticles, in conjunction with existing treatment technologies, can offer tremendous potential for the effective treatment of water and wastewater. Due to their unique properties related to magnetism and their surface and structural properties, these adsorption materials offer many alternative applications in many other fields. Their use has been growing in recent years, particularly in the recycling of critical materials—including rare-earth elements, which are now used in all high-tech products and are almost impossible to replace because their properties are unique or “rare”, which is why they are so highly valued, and their extraction and production pose major problems in terms of environmental pollution. In addition, such functionalized magnetic nanoparticles could also be effectively used to remove organic and biological pollutants such as organic dyes, fluoridated and chlorinated organic compounds, pesticides, bioactive compounds, etc., which are often found in groundwater, drinking water, and wastewater.

Despite the vast potential shown by functionalized magnetic nanomaterials as adsorbents, most of them are still at the laboratory research stage. The lack of legislation and regulation and the issue of toxicity of nanomaterials, which should also not be ignored, represent the major obstacles encountered in the remediation of water and wastewater with nanomaterials, while many other obstacles associated with their use are only temporary, such as high costs and technical handling.

Although many studies have been carried out on the adsorption of heavy metal ions, the mechanism of their interaction with adsorbents is, in many cases, not fully understood. Therefore, more research on the interactions between functionalized magnetic nanomaterials and pollutants is expected in the future, as they are of key importance for the design and improvement of the properties of adsorbents, but the lack of knowledge on their environmental and human impacts has to be taken into account in order to move towards a justification of their use in real environments.

Author Contributions: Conceptualization, A.L. and A.K.; Methodology, M.B. and A.K.; Validation, A.L.; Formal analysis, M.B., A.L. and A.K.; Investigation, A.L. and A.K.; Resources, N.D.; Data curation, M.L. and A.K.; Writing—original draft, M.B.; Writing—review & editing, A.F.P.A.M.R. and A.K.; Supervision, A.L. and A.K.; Project administration, A.L. and A.K.; Funding acquisition, A.L. All authors have read and agreed to the published version of the manuscript.

Funding: The project HMRcycle (E! 113543) has received funding from the Eurostars-2 joint program. We express our gratitude to the national funding organization—the Slovenian Ministry of Economic Development and Technology (MEDT)—for co-financing the project HMRcycle. This work is also supported by an international research project—the Marie Skłodowska-Curie Action “Global Mercury Observation and Training Network in Support to the Minamata Convention”, financed under the funding line “excellent science” of the Horizon 2020 research and innovation program of the European Commission under the Marie Skłodowska-Curie grant agreement no. 860497. The results were obtained within the Research program “Design of New Properties of (Nano)materials and Applications”, No. P2-0424, and the authors acknowledge the financial support from the Slovenian Research Agency. This research was also funded by the Ministry of Education, Science and Sport, Republic of Slovenia, and by the European Union through the European Regional Development Fund (ERDF), Early Research Careers 2.1 (Contract No. C3330-19-952032).

Institutional Review Board Statement: Not applicable.

Informed Consent Statement: Not applicable.

Conflicts of Interest: The authors declare that they have no conflict of interest.

References

1. Auerbach, R.; Bokelmann, K.; Stauber, R.; Gutfleisch, O.; Schnell, S.; Ratering, S. Critical raw materials—Advanced recycling technologies and processes: Recycling of rare earth metals out of end-of-life magnets by bioleaching with various bacteria as an example of an intelligent recycling strategy. *Miner. Eng.* **2019**, *134*, 104–117. [CrossRef]
2. European Commission; Blengini, G.; Latunussa, C.; Eynard, U.; Matos, C.; Georgitzikis, K.; Pavel, C.; Carrara, S.; Mancini, L.; Unguru, M.; et al. *Study on the EU's List of Critical Raw Materials (2020)*; Factsheets on Critical Raw Materials; Final Report; European Commission: Luxembourg, 2020. [CrossRef]
3. European Commission. *Critical Raw Materials for Strategic Technologies and Sectors in the EU, A Foresight Study*; European Commission: Luxembourg, 2020; ET-04-20-034-EN-N; ISBN 978-92-76-15336-8. [CrossRef]
4. Skirrow, R.G.; Huston, D.L.; Mernagh, T.P.; Thorne, J.P.; Dulfer, H.; Senior, A.B. *Critical Commodities for a High-Tech World: Australia's Potential to Supply Global Demand*; Geoscience Australia: Canberra, Australia, 2013.
5. Huang, H.; Wang, Y.; Zhang, Y.; Niu, Z.; Li, X. Amino-functionalized graphene oxide for Cr (VI), Cu (II), Pb (II) and Cd (II) removal from industrial wastewater. *Open Chem.* **2020**, *18*, 97–107. [CrossRef]
6. Girtan, M.; Wittenberg, A.; Grilli, M.L.; de Oliveira, D.P.S.; Giosuè, C.; Ruello, M.L. The Critical Raw Materials Issue between Scarcity, Supply Risk, and Unique Properties. *Materials* **2021**, *14*, 1826. [CrossRef] [PubMed]
7. Agency for Toxic Substances and Disease Registry (ATSDR). The Priority List of Hazardous Substances. Available online: <https://www.atsdr.cdc.gov/spl/index.html#2019spl> (accessed on 30 August 2022).
8. Reddy, D.H.K.; Yun, Y.-S. Spinel ferrite magnetic adsorbents: Alternative future materials for water purification. *Coord. Chem. Rev.* **2016**, *315*, 90–111. [CrossRef]
9. Carolin, C.F.; Kumar, P.S.; Saravanan, A.; Joshiba, G.J.; Naushad, M. Efficient techniques for the removal of toxic heavy metals from aquatic environment: A Review. *J. Environ. Chem. Eng.* **2017**, *5*, 2782–2799. [CrossRef]
10. Shrestha, R.; Ban, S.; Devkota, S.; Sharma, S.; Joshi, R.; Tiwari, A.P.; Kim, H.Y.; Joshi, M.K. Technological trends in heavy metals removal from industrial wastewater: A review. *Resour. Conserv. Recycl.* **2020**, *156*, 105688. [CrossRef]
11. Zhang, Y.; Wang, Y.; Zhang, H.; Li, Y.; Zhang, Z.; Zhang, W. Recycling spent lithium-ion battery as adsorbents to remove aqueous heavy metals: Adsorption kinetics, isotherms, and regeneration assessment. *J. Environ. Chem. Eng.* 2021, in press. [CrossRef]
12. Dhiman, V.; Kondal, N. ZnO Nanoadsorbents: A potent material for removal of heavy metal ions from wastewater. *Colloid Interface Sci. Commun.* **2021**, *41*, 100380. [CrossRef]
13. Fu, X.; Feng, X.; Sommar, J.; Wang, S. A review of studies on atmospheric mercury in China. *Sci. Total Environ.* **2012**, *421*–*422*, 73–81. [CrossRef]
14. Mousavi, A.; Chávez, R.D.; Ali, A.-M.S.; Cabaniss, S.E. Mercury in natural waters: A mini-review. *Environ. Forensics* **2011**, *12*, 14–18. [CrossRef]
15. Wang, J.; Feng, X.; Anderson, C.W.N.; Xing, Y.; Shang, L. Remediation of mercury contaminated sites—A review. *J. Hazard. Mater.* **2012**, *221*–*222*, 1–18. [CrossRef]
16. Tuzen, M.; Soylak, M. Mercury contamination in mushroom samples from Tokat, Turkey. *Bull. Environ. Contam. Toxicol.* **2005**, *74*, 968–972. [CrossRef] [PubMed]
17. Hu, H.; Lin, H.; Zheng, W.; Tomanicek, S.J.; Johs, A.; Feng, X.; Elias, D.A.; Liang, L.; Gu, B. Oxidation and methylation of dissolved elemental mercury by anaerobic bacteria. *Nat. Geosci.* **2013**, *6*, 751–754. [CrossRef]
18. Unceta, N.; Seby, F.; Malherbe, J.; Donard, O.F.X. Chromium speciation in solid matrices and regulation: A review. *Anal. Bioanal. Chem.* **2010**, *397*, 1097–1111. [CrossRef] [PubMed]
19. Calik, S.; Sözüdogru, O.; Massara, T.M.; Yilmaz, A.E.; Bakirdere, S.; Katsou, E.; Komesli, O.T. Removal of heavy metals by a membrane bioreactor combined with activated carbon. *Anal. Lett.* **2020**, *54*, 1616–1626. [CrossRef]
20. Henze, M.; Comeau, Y. Wastewater characterization. In *Biological Wastewater Treatment: Principles Modelling and Design*; IWA Publishing: London, UK, 2008; pp. 33–52.
21. Crini, G.; Lichtfouse, E. Advantages and disadvantages of techniques used for wastewater treatment. *Environ. Chem. Lett.* **2019**, *17*, 145–155. [CrossRef]
22. Chen, Q.; Yao, Y.; Lia, X.; Lu, J.; Zhou, J.; Huang, Z. Comparison of heavy metal removals from aqueous solutions by chemical precipitation and characteristics of precipitates. *J. Water Process Eng.* **2018**, *26*, 289–300. [CrossRef]
23. Delil, A.D.; Köleli, N.; Dağhan, H.; Bahçeci, G. Recovery of heavy metals from canola (*Brassica napus*) and soybean (*Glycine max*) biomasses using electrochemical process. *Environ. Technol. Innov.* **2020**, *17*, 100559. [CrossRef]
24. Dong, L.; Hou, L.; Wang, Z.; Gu, P.; Chen, G.; Jiang, R. A new function of spent activated carbon in BAC process: Removing heavy metals by ion exchange mechanism. *J. Hazard. Mater.* **2018**, *359*, 76–84. [CrossRef]
25. Bauman, M.; Košak, A.; Lobnik, A.; Petrinčić, I.; Luxbacher, T. Nanofiltration membranes modified with alkoxysilanes: Surface characterization using zeta-potential. *Colloids Surf. A Physicochem. Eng. Asp.* **2013**, *422*, 110–117. [CrossRef]
26. Peydayesh, M.; Mohammadi, T.; Nikouzad, S.K. A positively charged composite loose nanofiltration membrane for water purification from heavy metals. *J. Membr. Sci.* **2020**, *611*, 118205. [CrossRef]

27. Hargreaves, A.J.; Vale, P.; Whelan, J.; Alibardi, L.; Constantino, C.; Dotro, G.; Cartmell, E.; Campo, P. Impacts of coagulation-flocculation treatment on the size distribution and bioavailability of trace metals (Cu, Pb, Ni, Zn) in municipal wastewater. *Water Res.* **2018**, *128*, 120–128. [[CrossRef](#)] [[PubMed](#)]
28. Sun, Y.; Zhou, S.; Pan, S.-Y.; Zhu, S.; Yu, Y.; Zheng, H. Performance evaluation and optimization of flocculation process for removing heavy metal. *Chem. Eng. J.* **2020**, *385*, 123911. [[CrossRef](#)]
29. Al-Qahtani, K.M. Water purification using different waste fruit cortexes for the removal of heavy metals. *J. Taibah Univ. Sci.* **2016**, *10*, 700–708. [[CrossRef](#)]
30. Singh, N.B.; Nagpal, G.; Agrawal, S. Rachna, Water purification by using Adsorbents: A Review. *Environ. Technol. Innov.* **2018**, *11*, 187–240. [[CrossRef](#)]
31. Gul, A.; Khaligh, N.G.; Julkapli, N.M. Surface modification of Carbon-Based Nanoadsorbents for the Advanced Wastewater Treatment. *J. Mol. Struct.* **2021**, *1235*, 130148. [[CrossRef](#)]
32. Kegl, T.; Ban, I.; Lobnik, A.; Košak, A. Synthesis and characterization of novel γ -Fe₂O₃.NH₄OH@SiO₂(APTMS) nanoparticles for dysprosium adsorption. *J. Hazard. Mater.* **2019**, *378*, 120764. [[CrossRef](#)]
33. Da'na, E.; Awad, A. Regeneration of spent activated carbon obtained from home filtration system and applying it for heavy metals adsorption. *J. Environ. Chem. Eng.* **2017**, *5*, 3091–3099. [[CrossRef](#)]
34. Tang, Y.; Liang, S.; Wang, J.; Yu, S.; Wang, Y. Amino-functionalized core-shell magnetic mesoporous composite microspheres for Pb (II) and Cd (II) removal. *J. Environ. Sci.* **2013**, *25*, 830–837. [[CrossRef](#)]
35. Ahmadi, A.; Heidarzadeh, S.; Mokhtari, A.R.; Darezereshki, E.; Harouni, H.A. Optimization of heavy metal removal from aqueous solutions by maghemite (γ -Fe₂O₃) nanoparticles using response surface methodology. *J. Geochem. Explor.* **2014**, *147*, 151–158. [[CrossRef](#)]
36. Qian, J.; Yang, T.; Zhang, W.; Lei, Y.; Zhang, C.; Ma, J.; Zhang, C. Preparation of NH₂-Functionalized Fe₂O₃ and Its Chitosan Composites for the Removal of Heavy Metal Ions. *Sustainability* **2019**, *11*, 5186. [[CrossRef](#)]
37. Duan, C.; Ma, T.; Wang, J.; Zhou, Y. Removal of heavy metals from aqueous solution using carbon-based adsorbents: A review. *J. Water Process Eng.* **2020**, *37*, 101339. [[CrossRef](#)]
38. Aguayo-Villarreal, I.A.; Bonilla-Petriciolet, A.; Muñiz-Valencia, R. Preparation of activated carbons from pecan nutshell and their application in the antagonistic adsorption of heavy metal ions. *J. Mol. Liq.* **2017**, *230*, 686–695. [[CrossRef](#)]
39. Kołodziejka, D.J.; Krukowska, P. Thomas. Comparison of sorption and desorption studies of heavy metal ions from biochar and commercial active carbon. *Chem. Eng. J.* **2017**, *307*, 353–363, ISSN 1385-8947. [[CrossRef](#)]
40. Lo, S.-F.; Wang, S.-Y.; Tsai, M.-J.; Lin, L.-D. Adsorption capacity and removal efficiency of heavy metal ions by Moso and Ma bamboo activated carbons. *Chem. Eng. Res. Des.* **2012**, *90*, 1397–1406. [[CrossRef](#)]
41. Sujatha, S.; Sivarethinamohan, R. A critical review of Cr (VI) ion effect on mankind and its amputation through adsorption by activated carbon. *Mater. Today Proc.* **2021**, *37*, 1158–1162. [[CrossRef](#)]
42. You, J.; Wang, L.; Zhao, Y.; Bao, W. A review of amino-functionalized magnetic nanoparticles for water treatment: Features and prospects. *J. Clean. Prod.* **2021**, *281*, 124668. [[CrossRef](#)]
43. Wang, J.; Zheng, S.; Shao, Y.; Liu, J.; Xu, Z.; Zhu, D. Amino-functionalized Fe₃O₄@SiO₂ core-shell magnetic nanomaterial as a novel adsorbent for aqueous heavy metals removal. *J. Colloid Interface Sci.* **2010**, *349*, 293–299. [[CrossRef](#)]
44. Zhao, Y.-G.; Shen, H.-Y.; Pan, S.-D.; Hu, M.-Q.; Xia, Q.-H. Preparation and characterization of amino-functionalized nano-Fe₃O₄ magnetic polymer adsorbents for removal of chromium (VI) ions. *J. Mater. Sci.* **2010**, *45*, 5291–5301. [[CrossRef](#)]
45. Yavuz, C.T.; Mayo, J.T.; Yu, W.W.; Prakash, A.; Falkner, J.C.; Yean, S.; Colvin, V.L. Low-Field Magnetic Separation of Monodisperse Fe₃O₄ Nanocrystals. *Science* **2006**, *314*, 964–967. [[CrossRef](#)]
46. Ritu, D. Ambashta, Mika Sillanpaa. Water purification using magnetic assistance: A review. *J. Hazard. Mater.* **2010**, *180*, 38–49. [[CrossRef](#)]
47. Mandel, K.; Hutter, F.; Gellermann, C.; Sextl, G. Modified Superparamagnetic Nanocomposite Microparticles for Highly Selective Hg(II) or Cu(II) Separation and Recovery from Aqueous Solutions. *ACS Appl. Mater. Interfaces* **2012**, *4*, 5633–5642. [[CrossRef](#)] [[PubMed](#)]
48. Kim, J.S.; Yoon, T.-J.; Yu, K.N.; Kim, B.G.; Park, S.; Kim, H.W.; Lee, K.H.; Park, S.B.; Lee, J.-K.; Cho, M.H. Toxicity and tissue distribution of magnetic nanoparticles in mice. *Toxicol. Sci.* **2006**, *89*, 338–347. [[CrossRef](#)] [[PubMed](#)]
49. Jane Cypriana, J.P.J.; Saigeetha, S.; Lavanya Agnes Angalene, J.; Samrot, A.V.; Suresh Kumar, S.; Ponniah, P.; Chakravarthi, S. Overview on toxicity of nanoparticles, its mechanism, models used in toxicity studies and disposal methods. *Biocatal. Agric. Biotechnol.* **2021**, *36*, 102117. [[CrossRef](#)]
50. Douglas, L.A.; Baugher Brigitta, M.; Baugher Collen, R.; Schneider Duane, A.; Rahimian, K. Substituent effects on the sol-gel chemistry of organotrialkoxysilanes. *Chem. Mater. Am. Chem. Soc.* **2000**, *12*, 3624–3632. [[CrossRef](#)]
51. Brinker, C.J.; Scherer, G.W. *Sol-Gel Science: The Physics and Chemistry of Sol-Gel Processing*; Academic Press: Cambridge, UK, 1990; ISBN 0-12-134970-5.
52. Osterholtz, F.D.; Pohl, E.R. Kinetics of the hydrolysis and condensation of organofunctional alkoxysilanes: A review. *J. Adhes. Sci. Technol.* **1992**, *6*, 127–149. [[CrossRef](#)]
53. Colilla, M.; Vallet-Regí, M. Biocompatibility, Surface Engineering, and Delivery of Drugs, Genes and Other Molecules. In *Comprehensive Biomaterials II*; Elsevier: Amsterdam, The Netherlands, 2017. [[CrossRef](#)]

54. Zhang, J.; Zhai, S.; Li, S.; Xiao, Z.; Song, Y.; An, Q.; Tian, G. Pb (II) removal of Fe₃O₄@SiO₂-NH₂ core-shell nanomaterials prepared via a controllable sol-gel process. *Chem. Eng. J.* **2013**, *215–216*, 461–471. [CrossRef]
55. Liu, Q.; Liu, Q.; Liu, B.; Hu, T.; Liu, W.; Yao, J. Green synthesis of tannin-hexamethyldiamine based adsorbents for efficient removal of Cr (VI). *J. Hazard. Mater.* **2018**, *352*, 27–35. [CrossRef]
56. Pradhan, D.; Sukla, L.B.; Sawyer, M.; Rahman, P.K.; Rahman, S.M. Recent bioreduction of hexavalent chromium in wastewater treatment: A review. *J. Ind. Eng. Chem.* **2017**, *55*, 1–20. [CrossRef]
57. Takeno, N. Atlas of Eh-pH Diagrams, Intercomparison of Thermodynamic Databases, Geological Survey of Japan Open File Report No. 419, National Institute of Advanced Industrial Science and Technology, Research Center for Deep Geological Environments. May 2005. Available online: <https://www.nrc.gov/docs/ML1808/ML18089A638.pdf> (accessed on 30 August 2022).
58. De Zoubov, N.; Pourbaix, M. Mercury. In *Atlas of Electrochemical Equilibria in Aqueous Solutions*; Pourbaix, M., Ed.; Section 15.3; Pergamon Press: Oxford, UK, 1966.
59. Baes, C.F.; Mesmer, R.E. *The Hydrolysis of Cations*, 2nd ed.; Kreiger: New York, NY, USA, 1986.
60. Kipton J Powell; Brown, P.L.; Byrne, R.H.; Gajda, T.; Hefter, G.; Sjöberg, S.; Wanner, H.; Hefter, G. Chemical Speciation of Environmentally Significant Heavy Metals with Inorganic Ligands, Part 1: The Hg²⁺-Cl⁻, OH⁻, CO₃²⁻, SO₄²⁻, and PO₄³⁻ Aqueous Systems. *Pure Appl. Chem.* **2005**, *77*, 739–800. [CrossRef]
61. Sun, M.; Li, P.; Jin, X.; Ju, X.; Yan, W.; Yuan, J.; Xing, C. Heavy metal adsorption onto graphene oxide, amino group on magnetic nanoadsorbents and application for detection of Pb (II) by strip sensor. *Food Agric. Immunol.* **2018**, *29*, 1053–1073. [CrossRef]
62. Li, X.; Wang, S.; Liu, Y.; Jiang, L.; Song, B.; Li, M.; Ding, Y. Adsorption of Cu(II), Pb(II), and Cd(II) ions from acidic aqueous solutions by diethylenetriaminepentaacetic acid-modified magnetic graphene oxide. *J. Chem. Eng. Data* **2017**, *62*, 407–416. [CrossRef]
63. Shahbazi, A.; Younesi, H.; Badiei, A. Functionalized SBA-15 mesoporous silica by Melamine-based dendrimer amines for adsorptive characteristics of Pb(II), Cu(II), and Cd(II) heavy metal ions in batch and fixed bed column. *Chem. Eng. J.* **2011**, *168*, 505–518. [CrossRef]
64. Zhao, G.; Ren, X.; Gao, X.; Tan, X.; Li, J.; Chen, C.; Wang, X. Removal of Pb(II) ions from aqueous solutions on few-layered graphene oxide nanosheets. *Dalton Trans.* **2011**, *40*, 10945–10952. [CrossRef] [PubMed]
65. Nassar, N.N. Rapid removal and recovery of Pb(II) from wastewater by magnetic nano adsorbents. *J. Hazard. Mater.* **2010**, *184*, 538–546. [CrossRef] [PubMed]
66. Jawed, A.; Saxena, V.; Pandey, L.M. Engineered nanomaterials and their surface functionalization for the removal of heavy metals: A review. *J. Water Process Eng.* **2020**, *33*, 101009. [CrossRef]
67. Naseem, T.; Durrani, T. The role of some important metal oxide nanoparticles for wastewater and antibacterial applications: A review. *Environ. Chem. Ecotoxicol.* **2021**, *3*, 59–75. [CrossRef]
68. Samrot, A.V.; Sahithya, C.S.; Selvarani, A.J.; Purayil, S.K.; Ponnaiah, P. A review on synthesis, characterization and potential biological applications of superparamagnetic iron oxide nanoparticles. *Curr. Res. Green Sustain. Chem.* **2021**, *4*, 100042. [CrossRef]
69. Shokrollahi, H. A review of the magnetic properties, synthesis methods and applications of maghemite. *J. Magn. Magn. Mater.* **2017**, *426*, 74–81. [CrossRef]
70. Yang, J.; Hou, B.; Wang, J.; Tian, B.; Bi, J.; Wang, N.; Li, X.; Huang, X. Nanomaterials for the Removal of Heavy Metals from Wastewater. *Nanomaterials* **2019**, *9*, 424. [CrossRef]
71. Yong-Mei, H.; Man, C.; Zhong-Bo, H. Effective removal of Cu (II) ions from aqueous solution by ami-no-functionalized magnetic nanoparticles. *J. Hazard. Mater.* **2010**, *184*, 392–399. [CrossRef]
72. Gallo-Cordova, A.; Morales, M.d.P.; Mazarío, E. Effect of the Surface Charge on the Adsorption Capacity of Chromium (VI) of Iron Oxide Magnetic Nanoparticles Prepared by Microwave-Assisted Synthesis. *Water* **2019**, *11*, 2372. [CrossRef]
73. Srikaow, A.; Butburee, T.; Pon-On, W.; Srihirin, T.; Uraisin, K.; Suttiponpanit, K.; Chaveanghong, S.; Smith, S.M. Efficient Mercury Removal at Ultralow Metal Concentrations by Cysteine Functionalized Carbon-Coated Magnetite. *Appl. Sci.* **2020**, *10*, 8262. [CrossRef]
74. Mandela, K.; Huttera, F. The magnetic nanoparticle separation problem. *Nano Today* **2012**, *7*, 485–487. [CrossRef]
75. Kegl, T.; Košak, A.; Lobnik, A.; Novak, Z.; Kralj, A.K.; Ban, I. Adsorption of rare earth metals from wastewater by nano-materials: A review. *J. Hazard. Mater.* **2019**, *378*, 120764. [CrossRef]
76. Bhatia, R.; Singh, R. A review on nanotechnological application of magnetic iron oxides for heavy metal removal. *J. Water Process Eng.* **2019**, *31*, 100845. [CrossRef]
77. Jainae, K.; Sukpirom, N.; Fuangswasdi, S.; Unob, F. Adsorption of Hg (II) from aqueous solutions by thiol-functionalized polymer-coated magnetic particles. *J. Ind. Eng. Chem.* **2015**, *23*, 273–278. [CrossRef]
78. Viltužnik, B.; Lobnik, A.; Košak, A. The removal of Hg (II) ions from aqueous solutions by using thi-ol-functionalized cobalt ferrite magnetic nanoparticles. *J. Sol-Gel Sci. Technol.* **2015**, *74*, 199–207. [CrossRef]
79. Chen, Z.; Geng, Z.; Zhang, Z.; Ren, L.; Tao, T.; Yang, R.; Guo, Z. Synthesis of Magnetic Fe₃O₄@C Nanoparticles Modified with-SO₃H and -COOH Groups for Fast Removal of Pb²⁺, Hg²⁺, and Cd²⁺ Ions. *Eur. J. Inorg. Chem.* **2014**, *2014*, 3172–3177. [CrossRef]
80. Marimón-Bolívar, W.; Tejada-Benítez, L.; Herrera, A.P. Removal of mercury (II) from water using magnetic nanoparticles coated with amino organic ligands and yam peel biomass. *Environ. Nanotechnol. Monit. Manag.* **2018**, *10*, 486–493. [CrossRef]

81. Maitlo, H.A.; Kim, K.-H.; Kumar, V.; Kim, S.; Park, J.-W. Nanomaterials-based treatment options for chromium in aqueous environments. *Environ. Int.* **2019**, *130*, 104748. [[CrossRef](#)] [[PubMed](#)]
82. Nicola, R.; Costisor, O.; Ciopec, M.; Negrea, A.; Lazau, R.; Ianasi, C.; Piciorus, E.-M.; Len, A.; Almásy, L.; Szerb, E.I.; et al. Silica-Coated Magnetic Nanocomposites for Pb²⁺ Removal from Aqueous Solution. *Appl. Sci.* **2020**, *10*, 2726. [[CrossRef](#)]
83. Kakavandi, B.; Kalantary, R.R.; Jafari, A.J.; Nasser, S.; Ameri, A.; Esrafil, A.; Azari, A. Pb (II) adsorption onto a magnetic composite of activated carbon and superparamagnetic Fe₃O₄ nanoparticles: Experimental and modeling study. *CLEAN–Soil Air Water* **2015**, *43*, 1157–1166. [[CrossRef](#)]
84. Tao, Y.; Zhang, C.; Lü, T.; Zhao, H. Removal of Pb(II) Ions from Wastewater by Using Polyethyleneimine-Functionalized Fe₃O₄ Magnetic Nanoparticles. *Appl. Sci.* **2020**, *10*, 948. [[CrossRef](#)]
85. Gutiérrez-López, D.N.; Flores-Alamo, M.C.; Carreño-de-León, M.C.; Solache-Rios, M.J. Removal of Pb (II) from aqueous solution by using microspheres of Zea mays rachis–sodium alginate by batch and column systems. *Water Supply* **2020**, *20*, 2133–2144. [[CrossRef](#)]
86. Luo, Q.; Liu, G.; Wang, L.; Wang, W.; Wang, Y.; Wang, H.; Xu, W. Efficient removal of lead ions from aqueous solution using C-TiO₂ adsorbent. *IOP Conf. Ser. Earth Environ. Sci.* **2021**, *865*, 012040. [[CrossRef](#)]
87. Zhang, J.; Lin, S.; Han, M.; Su, Q.; Xia, L.; Hui, Z. Adsorption Properties of Magnetic Magnetite Nanoparticle for Coexistent Cr (VI) and Cu (II) in Mixed Solution. *Water* **2020**, *12*, 446. [[CrossRef](#)]
88. Hu, J.; Chen, G.; Lo, I.M.C. Removal and recovery of Cr (VI) from wastewater by maghemite nanoparticles. *Water Res.* **2005**, *39*, 4528–4536. [[CrossRef](#)]
89. Baghani, A.N.; Mahvi, A.H.; Gholami, M.; Rastkari, N.; Delikhoon, M. One-Pot synthesis, characterization and adsorption studies of amine-functionalized magnetite nanoparticles for removal of Cr (VI) and Ni (II) ions from aqueous solution: Kinetic, isotherm and thermodynamic studies. *J. Environ. Health Sci. Eng.* **2016**, *14*, 11. [[CrossRef](#)]
90. Trang, V.T.; Tam, L.T.; van Quy, N.; Phan, V.N.; van Tuan, H.; Huy, T.Q.; Dinh, N.X.; Le, A.-T. Enhanced adsorption efficiency of inorganic chromium (VI) ions by using carbonencapsulated hematite nanocubes. *J. Sci. Adv. Mater. Devices* **2020**, *5*, 392–399. [[CrossRef](#)]
91. Puzzkarewicz, A.; Kaleta, J. Chromium (VI) Adsorption on Modified Activated Carbons. *Appl. Sci.* **2019**, *9*, 3549. [[CrossRef](#)]
92. Bafroee, A.A.T.; Panahi, H.A.; Moniri, E.; Miralinaghi, M.; Hasani, A.H. Removal of Hg²⁺ by carboxyl-terminated hyperbranched poly(amidoamine) dendrimers grafted superparamagnetic nanoparticles as an efficient adsorbent. *Environ. Sci. Pollut. Res.* **2020**, *27*, 9547–9567. [[CrossRef](#)] [[PubMed](#)]
93. Wang, Z.; Wu, D.; Wu, G.; Yang, N.; Wu, A. Modifying Fe₃O₄ microspheres with rhodamine hydrazide for selective detection and removal of Hg²⁺ ion in water. *J. Hazard. Mater.* **2013**, *244–245*, 621–627. [[CrossRef](#)] [[PubMed](#)]
94. Pan, S.; Shen, H.; Xu, Q.; Luo, J.; Hu, M. Surface mercapto engineered magnetic Fe₃O₄ nanoadsorbent for the removal of mercury from aqueous solutions. *J. Colloid Interface Sci.* **2012**, *365*, 204–212. [[CrossRef](#)]
95. Morsi, R.E.; Al-Sabagh, A.M.; Moustafa, Y.M.; ElKholi, S.G.; Sayed, M.S. Polythiophene modified chitosan/magnetite nanocomposites for heavy metals and selective mercury removal. *Egyptian J. Pet.* **2018**, *27*, 1077–1085. [[CrossRef](#)]
96. Chen, D.; Awut, T.; Liu, B.; Ma, Y.; Wang, T.; Nurulla, I. Functionalized magnetic Fe₃O₄ nanoparticles for removal of heavy metal ions from aqueous solutions. *E-Polym.* **2016**, *16*, 313–322. [[CrossRef](#)]
97. Hao, Y.; Pan, Y.; Du, Q.; Li, X.; Wang, X. Nanoparticle Fe₃O₄ magnetized activated carbon from *Armeniaca sibirica* shell for the adsorption of Hg(II) ions. *BioResources* **2021**, *16*, 6100–6120. [[CrossRef](#)]
98. Zhang, X.; Hao, Y.; Wang, X.; Chen, Z.; Li, C. Competitive Adsorption of Cadmium(II) and Mercury(II) Ions from Aqueous Solutions by Activated Carbon from *Xanthoceras sorbifolia* Bunge Hull. *J. Chem.* **2016**, 4326351. [[CrossRef](#)]
99. Sereshti, H.; Gaikani, H.; Rashidi Nodeh, H. The effective removal of mercury ions (Hg²⁺) from water using cadmium sulfide nanoparticles doped in polycaprolactam nanofibers: Kinetic and equilibrium studies. *J. Iran. Chem. Soc.* **2018**, *15*, 743–751. [[CrossRef](#)]
100. Cullity, B.D.; Stock, S.R. *Elements of X-Ray Diffraction*, 3rd ed.; Prentice-Hall Inc.: Hoboken, NJ, USA, 2001; pp. 96–102. ISBN 0-201-61091-4.
101. Patterson, A. The Scherrer Formula for X-Ray Particle Size Determination. *Phys. Rev.* **1939**, *56*, 978–982. [[CrossRef](#)]
102. Pérez-Quintanilla, D.; del Hierro, I.; Fajardo, M.; Sierra, I. Mesoporous silica functionalized with 2-mercaptopyridine: Synthesis, characterization and employment for Hg (II) adsorption. *Microporous Mesoporous Mater.* **2006**, *89*, 58–68. [[CrossRef](#)]
103. Pérez-Quintanilla, D.; del Hierro, I.; Fajardo, M.; Sierra, I. 2-Mercaptothiazoline modified mesoporous silica for mercury removal from aqueous media. *J. Hazard. Mater.* **2006**, *134*, 245–256. [[CrossRef](#)] [[PubMed](#)]
104. Pérez-Quintanilla, D.; del Hierro, I.; Fajardo, M.; Sierra, I. Preparation of 2-mercaptobenzothiazole-derivatized mesoporous silica and removal of Hg (II) from aqueous solution. *J. Environ. Monit.* **2006**, *8*, 214–222. [[CrossRef](#)] [[PubMed](#)]
105. Liang, R.; Zou, H. Removal of aqueous Hg (II) by thiol-functionalized nonporous silica microspheres prepared by one-step sol-gel method. *RSC Adv.* **2020**, *10*, 18534–18542. [[CrossRef](#)] [[PubMed](#)]
106. Atul Kumar, M.; Sharma, A.; Maurya, I.K.; Thakur, A.; Kumar, S. Synthesis of ultra-small iron oxide and doped iron oxide nanostructures and their antimicrobial activities. *J. Taibah Univ. Sci.* **2019**, *13*, 280–285. [[CrossRef](#)]
107. Smith, B. *Infrared Spectral Interpretation, A Systematic Approach*; CRC Press: Boca Raton, FL, USA, 1999; 288p.

108. Sing, K.S.W.; Everett, D.H.; Haul, R.A.W.; Moscou, L.; Pierotti, R.A.; Rouquerol, J.; Siemieniowska, T. Reporting Physisorption Data for Gas-Solid Systems with Special Reference to the Determination of Surface-Area and Porosity. *Pure Appl. Chem.* **1985**, *57*, 603. [[CrossRef](#)]
109. Rouquerol, F.; Rouquerol, J.; Sing, K. *Adsorption by Powders and Porous Solids*; Academic Press: San Diego, CA, USA, 1999; ISBN 0-12-598920-2.
110. Zasonska, B.A.; Liškova, A.; Kuricova, M.; Tulinska, J.; Pop-Georgievski, O.; Čiampor, F.; Vavra, I.; Dušinska, M.; Ilavska, S.; Horvathova, M.; et al. Functionalized porous silica@magnetite core-shell nanoparticles for applications in medicine: Design, synthesis, and immunotoxicity. *Croat. Med. J.* **2016**, *57*, 165–178. [[CrossRef](#)]
111. Sun, M.; Cheng, G.; Ge, X.; Chen, M.; Wang, C.; Lou, L.; Xu, X. Aqueous Hg (II) immobilization by chitosan stabilized magnetic iron sulfide nanoparticles. *Sci. Total Environ.* **2018**, *621*, 1074–1083. [[CrossRef](#)]
112. Roy, A.; Bhattacharya, J. *Nanotechnology in Industrial Wastewater Treatment*; IWA Publishing: Durham, NC, USA, 2014; Volume 13. [[CrossRef](#)]
113. Dinker, M.K.; Kulkarni, P.S. Recent Advances in Silica-Based Materials for the Removal of Hexavalent Chromium: A Review. *J. Chem. Eng. Data* **2015**, *60*, 2521–2540. [[CrossRef](#)]
114. Alqadami, A.; Naushad, M.; Abdalla, M.A.; Anhamad, T.; Alothman, Z.A.; Alshehri, S.M. Synthesis and characterization of Fe₃O₄@TSC nanocomposite: Highly efficient removal of toxic metal ions from aqueous medium. *RSC Adv.* **2016**, *6*, 22679–22689. [[CrossRef](#)]
115. Gallios, G.P.; Vaclavikova, M. Removal of chromium (VI) from water streams: A thermodynamic study. *Environ. Chem. Lett.* **2008**, *6*, 235–240. [[CrossRef](#)]
116. Ghasemi, Z.; Seif, A.; Ahmadi, T.S.; Zargar, B.; Rashidi, F.; Rouzbahani, G.M. Thermodynamic and kinetic studies for the adsorption of Hg (II) by nano-TiO₂ from aqueous solution. *Adv. Powder Technol.* **2012**, *23*, 148–156. [[CrossRef](#)]
117. López-Muñoz, M.J.; Arencibia, A.; Cerro, L.; Pascual, R.; Melgar, Á. Adsorption of Hg (II) from aqueous solutions using TiO₂ and titanate nanotube adsorbents. *Appl. Surf. Sci.* **2016**, *367*, 91–100. [[CrossRef](#)]